Novel methods for 3-D semi-automatic mapping of fracture geometry at exposed rock faces

Quanhong Feng

Stockholm, Sweden, 2001

Doctoral Thesis
Division of Engineering Geology
Department of Civil and Environmental Engineering
Royal Institute of Technology

Doctoral Thesis

Novel methods for 3-D semi-automatic mapping of fracture geometry at exposed rock faces

by

Quanhong Feng

封 全 宏

Division of Engineering Geology
Department of Civil and Environmental Engineering
Royal Institute of Technology
S-100 44, Stockholm, Sweden

May, 2001

To Guojuan, Yan, Jesse
and
our families

FOREWORD:

The research work presented in this thesis was conducted in 1997 – 2001 at Division of Engineering Geology, Department of Civil and Environmental Engineering, Royal Institute of Technology (KTH). During this period, many people have helped me in one way or another. To all of them, I would like to express my utmost gratitude.

First of all, I wish to express my sincere gratitude to my supervisor Professor Ove Stephansson, Division of Engineering Geology, KTH, for his supervision, encouragement and enthusiastic support, and especially for his trust and interest in this work.

I am also deeply grateful to my assistant supervisor Senior lecturer Anders Boberg, Division of Photogrammetry, KTH, for introducing me to the field of photogrammetry. His advice and valuable suggestions on this thesis work are very much appreciated.

I would also like to take this chance to thank Beijing Research Institute of Geology (BRIG), P.R. China, for giving me permission to pursue this study in Sweden.

Financial support from the Axel and Margaret Ax:son Johnson Foundation, Stockholm is gratefully acknowledged.

I would like to express my special thanks to Dr. Kennert Röshoff at BBK AB, Sweden, and Dr. Christoph Fröhlich, Mr. Jörg Meixner, Mr. Markus Mettenleiter, Mr. Franz Härtl at Zoller + Fröhlich GmbH, Germany, for their help to use the 3-D laser scanner (LARA). Many thanks to Mr. Sven Vejde at SBG AB, Sweden for his kind help and sharing his software, equipment and surveying knowledge. Sincere thanks to Mr. Åke Bollö at Leica Geosystem, AB, and Mr. Svein Nilsen at Spectra Precision AB, Stockholm, for their kind help to use the non-reflector total station and associated programs. I am also very grateful to Professor Kennert Torlegård, Senior lecturer Anders Boberg, Dr. Peter Axelsson and Mr. Jonas Nelson at Division of Photogrammetry, KTH, for sharing their photogrammetry knowledge about the secret of 3-D mapping from images. Thanks to Senior lecturer Fan Huaan and Dr. Milan Horemuz at Division of Geodesy, KTH, for sharing their geodesy knowledge and other kind help. Thanks To Dr. Anders Fredriksson and Mr. Mikael Creütz at Golder Associates, Stockholm, for their help on scanning the rock face. And thanks to Drs. Weixing Wang and Fredrik Bergholm for sharing their knowledge on image processing and other related kind help.

I would like to extend my special thanks to Docent Lanru Jing and Senior lecturer Joanne Fernlund for their suggestions and comments on the manuscripts of my papers and thesis.

Thanks to Ph.D. student Nader Fardin for our successful co-operation on Paper E. Thanks also to Mr. Peter Sjögren, former MSc. Student, for his kind help and co-operation in collecting the field data at the beginning of this work.

In particular, I would like to thank Ulla Engberg for her kind help in different ways. Further thanks to all my fellow graduate students, both former and present, for creating a friendly and stimulating working environments, and for all the contribution to my thesis work with their assistance, advice, interesting and friendship. Thanks to all my friends for their help in one way or another.

Last but not least, I owe my dearest thanks to my wife Guojuan for her patience and encouragement during the period of this study, and to my two sons Yan and Jesse for their understanding of my busy work.

ABSTRACT

To analyse the influence of fractures on hydraulic and mechanical behaviour of fractured rock masses, it is essential to characterise fracture geometry at exposed rock faces. This thesis describes three semi-automatic methods for measuring and quantifying geometrical parameters of fractures, and aims to offer a novel approach to the traditional mapping methods.

Three techniques, i.e. geodetic total station, close-range photogrammetry and 3-D laser scanner, are used in this study for measurement of fracture geometry. The advantages of these techniques compared with the traditional method are: i) fracture geometry is quantified semi-automatically in three dimensions; ii) fracture measurements are obtained without physically touching the rock face; iii) the accuracy of fracture measurements is improved comparing with the traditional method; iv) both quantitative and spatial analysis of fracture geometry is possible; v) it offers a way to digitally record the rock surface in three dimensions and in visual format as a database for other applications.

The common approach for fracture mapping by using the novel techniques comprises three main steps: i) capturing 3-D co-ordinates of target points; ii) quantifying geometrical parameters of fractures from the recorded co-ordinates; iii) documenting the results of fracture mapping. The details of capturing 3-D co-ordinates of target points are introduced. A new algorithm is developed for computing orientation of fracture planes. A multiple approach for documenting the fracture mapping results is presented. Application of these techniques for measuring and quantifying the geometrical parameters of fractures, such as orientation, trace length and surface roughness, are demonstrated.

The presented methods can greatly improve the quality of fracture measurements and avoid the drawbacks inherent in traditional methods. However, it can not replace the human capacity to filter out and interpret the large amount of geometrical information displayed on the rock faces. The methods may offer an assistance to engineers or geologists in obtaining as much information as possible about the geometry and orientation of rock fractures for rock engineering applications.

Keywords: 3-D laser scanner, close-range photogrammetry, engineering geology, fracture geometry, fracture mapping, rock engineering, rock faces, rock mechanics, three-dimension, total station.

PREFACE

This doctoral thesis summarizes the work presented in the following appended papers:

Paper A.
Feng Q., Sjögren P., Stephansson O. and Jing L (2001). Measuring fracture orientation at exposed rock faces by using a non-reflector total station. Engineering Geology 59, pp. 133-146.

Paper B.
Feng Q., Boberg A. and Stephansson O. (2001). Fracture mapping at exposed rock faces by using close range digital photogrammetry and geodetic total station. Proceedings of the 38th USA Rock Mechanics Symposium, Washington DC, USA. Balkema, Rotterdam. (in press).

Paper C.
Feng Q., Mettenleiter M. Jing L. and Stephansson O. (2001). 3-D mapping of fracture geometry at exposed rock faces by using Laser Radar. Submitted for publication in International Journal of Rock Mechanics and Mining Sciences.

Paper D.
Feng Q. (2000). An algorithm for determining orientation parameters of rock fractures. Submitted for publication in Computers & Geosciences.

Paper E.
Feng Q., Fardin N., Jing L. and Stephansson O. (2001). A new method for *in-situ* non-contact measurement of large-scale fracture roughness. Submitted for publication in International Journal of Rock Mechanics and Mining Sciences.

Paper F.
Feng Q., Jing L., Stephansson O. and Vejde S. (2001). A new approach for geological surveying of exposed rock faces. Proceedings of the 2nd Asian Rock Mechanics Symposium, Beijing, China. Balkema, Rotterdam. (in press).

CONTENTS

1. Introduction

Rock masses are mostly composed of two major components: i) blocks of intact rocks; and ii) mechanical cracks termed as fractures or discontinuities. The hydromechanical behaviour of fractured rock masses depends mostly on the features of fractures. One of the most important tasks in rock engineering is to understand and analyse the influence of fractures on the rock construction, such as tunnels, mines, slopes, underground excavations and nuclear waste repositories. The success of a rock engineering project mostly depends on how well the fractures are characterised and considered in the design and construction.

To investigate the influence of fractures, the fundamental work is to measure and observe geometrical characteristics of fractures from either boreholes or exposed rock faces. Until recently, fracture mapping at exposed rock faces was conducted in a subjective way by using the traditional tools such as a compass with inclinometer, measuring tapes and a roughness profile gauge. The drawbacks inherent in the traditional method have great impact on the quantity and quality of fracture data, and will inevitably affect our understanding of the influence of fractures on the rock mass behaviour. The work presented in this thesis aims to apply new techniques for more efficient characterisation of fracture geometry at exposed rock faces.

1.1 Fracture geometry to be characterised at exposed rock faces

Fracture or discontinuity is a general term used in rock engineering to describe all mechanical breaks, either geological-origin or man-made, such as faults, joints, cracks, bedding planes and contacts. To characterise the features of fractures from exposed rock faces, the International Society for Rock Mechanics (ISRM) proposed ten parameters [1],

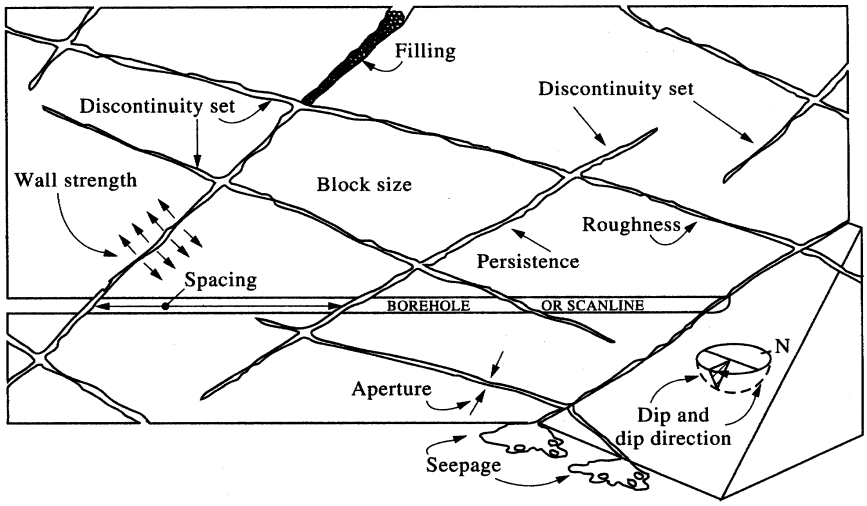

Figure 1. Primary geometrical properties of discontinuities in rock (from Hudson [2])

namely: orientation, spacing, persistence (or trace length), roughness, aperture, wall strength, filling, seepage, number of fractures sets, and block size (shown in Figure 1), to describe the geometrical, mechanical and hydraulic features of fractures. These parameters are briefly described below.

1) *Orientation* is the attitude of a fracture in space. It can be described by dip angle, dip direction and strike (see Figure 2).

- *Dip angle (DA)* is the angle between the fracture plane and the horizontal plane;
- *Dip direction (DD)* is the angle in the horizontal plane counted clockwise from the true North to the steepest declination line of the fracture plane (or the azimuth of the steepest declination line of a fracture plane);
- *Strike* actually refers to the two directions of a line that is intersected by the fracture plane and the horizontal plane. In geological mapping, strike indicates one of two directions of the intersection line. The relationship between the strike direction and the dip direction often follows the right-hand rule, which means the dip direction is pointing to one's right side when one is standing along the strike line and facing to the strike direction. In this case, Dip direction = Strike + 90°.

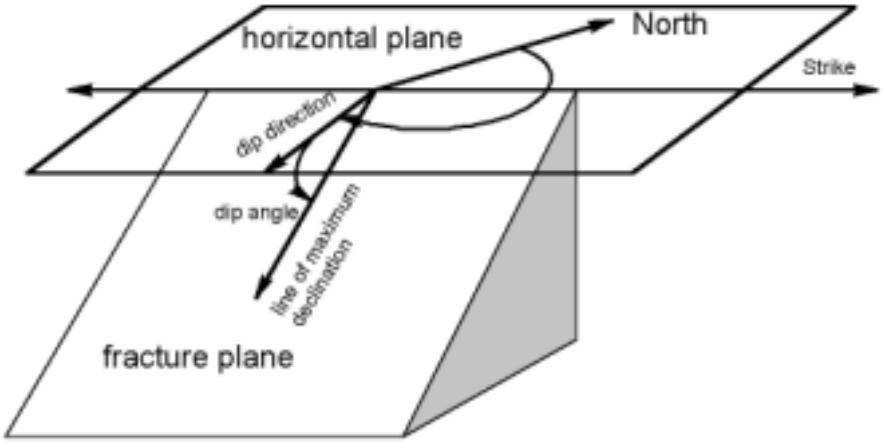

Figure 2. Definition of orientation parameters of a fracture plane.

2) *Spacing* is defined, in a general sense, as the distance between fractures (Figure 3). But in rock engineering it might refer to three different types of fracture spacings [3]:

- *Total spacing* is the spacing between a pair of immediately adjacent fractures, measured along a line of general, but specified location and orientation.
- *Set spacing* is the spacing between a pair of immediately adjacent fractures from a particular fracture set, measured along a line of any specified location and orientation.
- *Normal set spacing* is the set spacing of fractures when measured along a line that is parallel to the mean normal to the set.

Fracture frequency is also an important parameter which refers to the number of fractures that are observed or predicted to occur in a unit volume, unit area or unit length of a sample from a given rock mass [3].

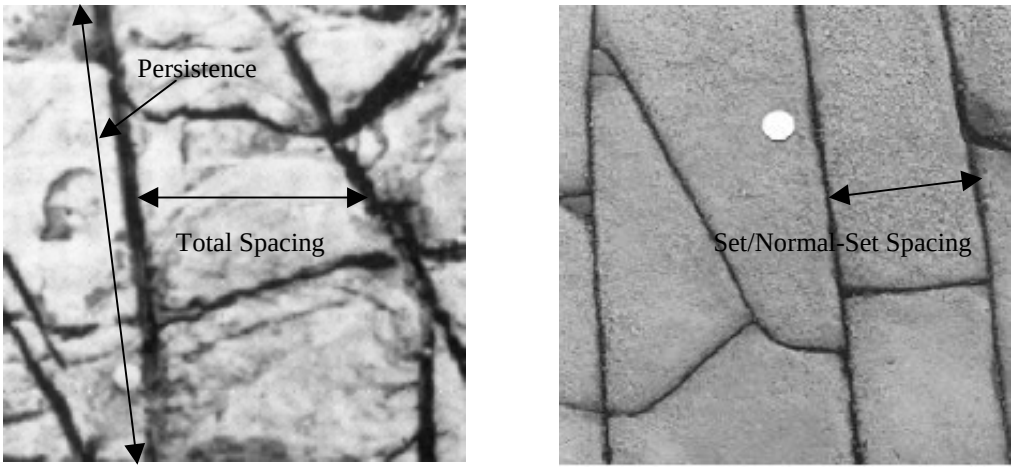

(a) (b)

Figure 3. Definition of spacing and persistence (after Reid and Harrison [4])

3) *Persistence (or trace length)* is the fracture trace length observed at a rock exposure.
4) *Roughness* refers to the inherent surface undulation and waviness relative to the mean plane of a fracture (Figure 4a).
5) *Aperture* is the perpendicular distance between adjacent rock walls of a fracture in which the intervening space is air or water filled (Figure 4b).

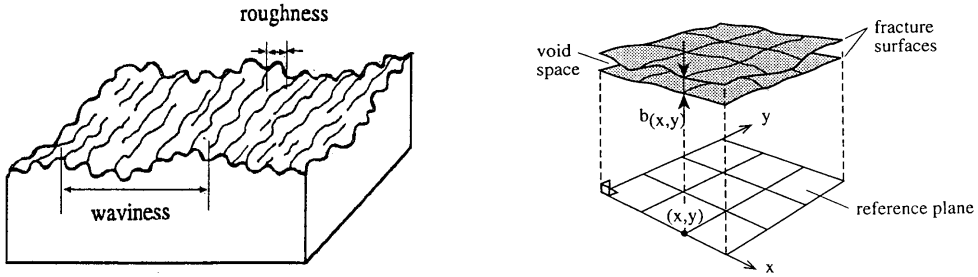

(a) (b)

Figure 4. Definition of (a) roughness and waviness (after Indraratna *et al* [5]), and (b) aperture (after Hakami [6]).

6) *Number of sets* is the number of fracture sets comprising the intersecting fracture system.
7) *Block size* refers to the rock block dimensions resulting from the mutual orientation of intersecting fracture sets and the spacing of the individual sets.
8) *Filling* refers to the material that separates the adjacent rock walls of a fracture.
9) *Wall strength* is the equivalent compression strength of the adjacent rock walls of a fracture.
10) *Seepage* refers to fluid flow and free moisture visible in individual fractures or in the rock mass as a whole.

To concentrate on the measurement of geometrical parameters of fractures, some of the parameters, including wall strength, filling and seepage, can be disregarded. Furthermore,

it can be argued that aperture, number of fracture sets and block size are not independent parameters, but related to or functions of orientation, spacing, persistence and roughness. In this case, fracture geometry in rock engineering applications can be considered as a four-parameter concept [7], and these four parameters are usually required to be measured when conducting fracture mapping at exposed rock faces.

1.2 State-of-the-art in rock fracture mapping

Fracture mapping comprise three steps as a whole procedure: i) capturing the fracture measurements in the field; ii) quantifying and analysing geometrical parameters of fractures; and iii) documenting and presenting the mapping results. Although the traditional methods are still mostly used in current rock engineering projects, a move towards employing new techniques to improve the fracture mapping quality and efficiency has been noted in recent years.

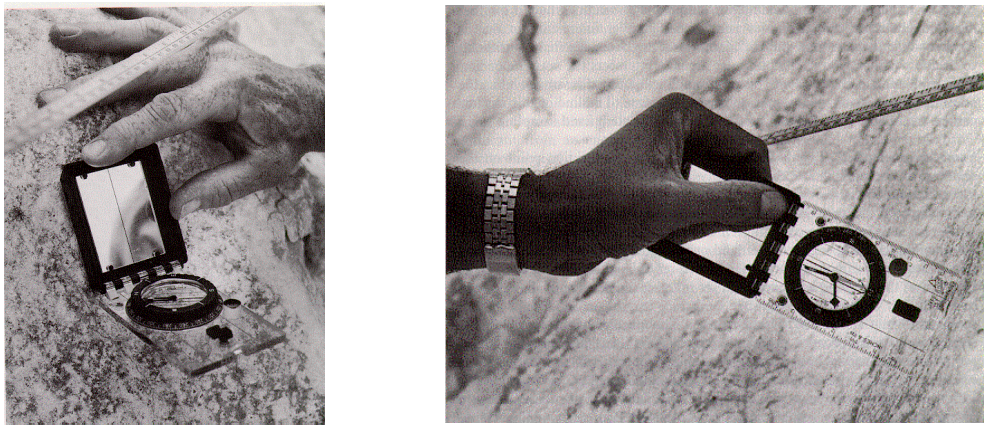

(a) (b)

Figure 5. Using a geological compass with inclinometer for measuring (a) dip direction and (b) dip angle (after Priest [3]).

Capturing fracture measurements from the exposed rock faces is the basis for other two subsequent procedures. Up to recently, the traditional methods are still mostly used to measure the fracture geometry in rock engineering projects. With the conventional method, orientation parameters, i.e. dip direction, strike and dip angle, of fracture surfaces are measured by using a geological compass and inclinometer (see Figure 5). The measuring tape is used to measure spacing and persistence (or trace length). Roughness and waviness are captured by using a roughness profile gauge (see Figure 6-1) [1], tangent plane and connected pin (see Figure 6-2) [8].

Fracture mapping by using these traditional tools will inevitably have some drawbacks, for instance:
i) The considerable personal contact with the rock face can lead to some drawbacks for collecting the measurements. Firstly, if the rock face is inaccessible or dangerous for reaching physically, the measurements might be missing. Secondly, too large part of the rock face can be out of the human reaching range.

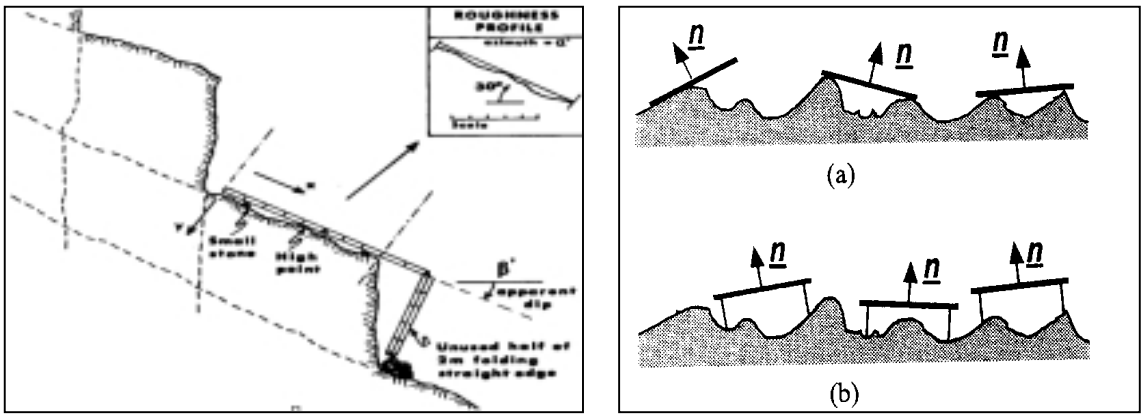

(1) (2)

Figure 6. Measuring roughness by using a roughness profile gauge (1) [1], tangent plane (2):(a) and connected pin (2):(b) [8].

ii) The intensive manual operation is time-consuming. Such as adjusting the compass in the correct position relative to true North when measuring dip direction or strike, determining where the compass can be put in order to obtain the true orientation of fracture planes, taking notes in the field notebook to record the measurements. Therefore, it is difficult to capture a large number of measurements in a short period of time.
iii) The measurements are captured in a subjective way because the fracture geometry is firstly observed and interpreted, and then measured in a way according to the operator's experience and geological knowledge. In addition, some of human limits might also affect the measurement accuracy. For example, when measuring fracture orientation, the steepest inclination of a fracture surface is difficult to determine by human's visualisation, which lends to the involvement of apparent orientations. A former study [9] has shown that the discrepancy of strike (or dip direction) measurements for shallow-dipping fractures (with dip angle less than 25 degrees [10]) can exceed 20 or 30 degrees even if the compass is repeatedly placed on the same spot. Therefore, the accuracy of measurements is uncertain.

To avoid the above disadvantages of the traditional method for fracture mapping, the efforts of developing new techniques for fracture mapping are in progress. The techniques such as photogrammetry, image processing, total station and laser scanner have been tried by several research groups and are briefly reviewed here.

Analytical photogrammetry techniques have been used for measuring fracture geometry at exposed rock faces by Harrison [7], Ross-Brown *et al*.[11] and Coe [12]. With this method, each pair of photo hard copies are used to create a stereoscopic view of target areas of the rock face by a stereoscopic plotter or stereocomparator. Geometrical parameters of fractures, such as orientation, spacing and trace length, can then be determined by capturing co-ordinates of several target points. With the latest development of digital photogrammetry technology, the procedure (similar to that of analytical photogrammetry) for capturing 3-D data can be conducted in the PC with a proper software by using a pair of digital images of rock faces, instead of hard copy

photos. This method has recently been applied for fracture mapping in tunnelling by Beer *et al*. [13].

Image processing has also been applied for fracture mapping. Since image processing techniques are widely applied to automatic operation in different industries, e.g. measuring geometry of rock aggregates [14], architecture and automobile production, several research groups have recently started to utilise image processing techniques for automatic measurement of fracture geometry. The research work done by Reid and Harrison [4], Hadjigeorgiou *et al.* [15], Post and Kemeny [16] have successfully applied different image segmentation techniques to automatically extract and recognise trace lines of fractures. Roughness measurement was also performed by using image processing technique [17]. To perform the automatic 3-D mapping, automatic image matching is another important step. Due to the complexity of the features of the rock face images, it seems now difficult to make a successful achievement for 3-D fracture mapping by image processing techniques.

Total station (TS) is a geodetic method usually used for surveying and mapping. It also has been employed for determining trace length of fractures on inaccessible rock slopes by Bulut and Tüdes [18]. With the TS method, the discontinuity traces can be determined by the co-ordinates of a set of points, but the co-ordinates of the points must be captured by the help of a reflector.

Laser scanner is another useful tool for 3-D mapping of fracture geometry. Ord and Cheung [19] described an automatic system for measuring the three-dimensional geometry of a rock face based on a planar laser technique. With this system, fracture orientation can be obtained in a relatively straightforward way. Estimation of fracture frequency, size, surface geometry and qualitative characteristics such as filling is also possible. Meanwhile, the 3-D laser scanner was also used to quantify roughness and aperture of fracture surfaces at laboratory scale [20, 21].

All of the above-mentioned efforts have improved the capturing of fracture geometry in the field, but they are now still not widely used in rock engineering projects. It might be due to the reasons such as cost of the equipment, lack of background knowledge and special training, and non-maturity of the techniques. In addition, some drawbacks of these methods could also affect the wide application of these techniques to rock engineering projects. For instance, 3-D measurements are difficult to extract by using image processing techniques; Laser scanner records all parts of a target area with a large amount of data, although only a few percent of the scanned data are needed for fracture mapping. For some scanners, the scanning speed is low for scanning the rock face, and it is not easy to filter out unusable information. Although photogrammetry is useful, it requires special photographic conditions to obtain a pair of photos for stereoscopic view mapping. The total station method used by Bulut and Tüdes [18] needs a reflector to be put at each target points on the rock face, which causes a problem to measure fracture geometry on inaccessible or dangerous rock faces.

1.3 Scope of this thesis

This thesis presents three methods, i.e. geodetic non-reflector total station (TS), close-range digital photogrammetry (CRDP), 3-D laser radar (LARA), for capturing 3-D co-ordinates of target points and quantifying geometrical parameters of fractures from the recorded co-ordinates. The purpose of this study is to apply some new techniques to the following three steps of fracture mapping: 1) capturing measurements of fracture geometry; 2) quantifying and analysing geometrical parameters of fractures; 3) and documenting the mapping results.

The four parameters of fracture geometry, i.e. orientation, spacing, trace length and roughness, have been semi-automatically measured at rock faces by the presented three methods in three dimensions and without physically touching the rock faces. By using the TS, a local 3-D co-ordinate system can be established and linked to a known global co-ordinate system if GPS (Global Positioning System) was used.

This thesis consists of a summary and six appended papers (Paper A-F). In the summary, following this introduction, 3-D mapping of fracture geometry by three novel methods are summarised from Paper A, B, C and E. The TS method was described in Paper A for measuring fracture orientation, and in Paper E for characterising the roughness of a large fracture surface. The accuracy of TS and some influential factors for fracture mapping are also discussed. Paper B presents the close-range digital photogrammetry method for fracture mapping. Different from the former work by other research groups, the convergent restitution techniques were applied in this study for measuring fracture geometry, so that more than two images of the rock faces can be used. The non-reflector TS was also used for capturing control points and establishing the object co-ordinate system. A new type of 3-D laser scanner, Laser Radar (LARA), was applied for fracture mapping in Paper C. By using LARA system, the rock faces can be quickly scanned with an acceptable accuracy, and both the co-ordinates and the reflectance intensity of each point are simultaneously recorded. Therefore, the 3-D co-ordinates of target points can be captured directly from the image of rock faces, and then fracture geometry can be quantified.

After describing these three methods, a new algorithm developed for computing fracture orientation (Paper D) is introduced. The techniques for documenting the results of fracture mapping are then presented. Paper F summarised three methods for fracture mapping and briefly described different steps of fracture mapping. Finally, the pros and cons on fracture mapping by three novel methods together with the traditional method are compared, results of this study are discussed, and conclusions of the thesis work are drawn, suggestions for the future work are also provided.

2. Geodetic total station method

This method has been presented in Paper A, E and the author's licentiate thesis [60]. In this Chapter, the main points of this method are summarised.

2.1 Geodetic total station

A total station (TS) is a geodetic instrument usually used for measuring the position of target points in space. It first appeared in the late 1980s as a result of the development of electronics and computerisation for surveying instrumentation [22]. With the rapid development of electronic engineering and computer technology in the 1990s, the TS is now undergoing a rapid refinement for its function and accuracy, and lowering of the cost. Therefore, the TS is now used by surveyors as a typical instrument to measure distances, angles and co-ordinates of target points. In this study, the non-reflector TS was employed as a tool, similar to a point-sensing laser scanner, to capture the 3D co-ordinates of the target points and to quantify the fracture geometry without physically touching the rock faces.

The TS is essentially an electronic theodolite that contains an integral electronic distance measurement instrument (EDM) with coaxial optics. The typical TS instrument consists of four main components: i) an EDM; ii) an electronic theodolite (ET); iii) a data collector; and iv) an on-board microprocessor [23].

Figure 7 schematically shows the measuring principle of the TS. The EDM is used to measure the slope distance of a target point P. The ET measures the horizontal and vertical angles of the point. From the measurements of angles and distances, the horizontal and vertical distances or the co-ordinates of the target point can be calculated with equation (1) by the on-board microprocessor in real time. The result is stored in the data collector. These raw data can be transferred to a computer for the use of any surveying-related applications.

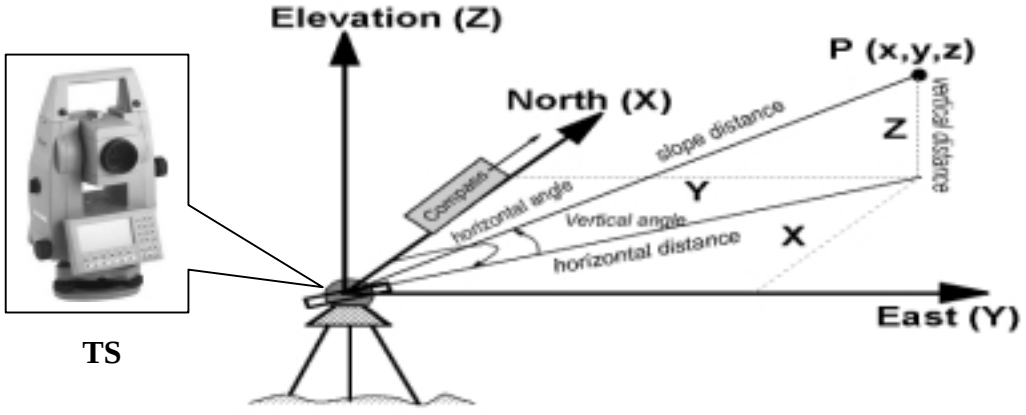

Figure 7. Definition of co-ordinates of a point within a local co-ordinate system

$$\left\{\begin{array}{l} X = S\cos(VA)\cos(HA) \\ Y = S\cos(VA)\sin(HA) \\ Z = S\sin(VA) \end{array}\right\} \quad (1)$$

where S = Slope distance, VA = Vertical Angle, HA = Horizontal Angle. The horizontal angle is determined with regard to true north, given by a compass or more accurately from measurements of control points with known geodetic co-ordinates.

The TS instruments can be categorised in two types, i.e. the reflector TS and the non-reflector TS, according to the measuring principle of the EDM. Current EDMs use either infrared light (light waves) or microwaves (radio waves). The microwave EDMs require a transmitter/receiver at both ends of the measured line, whereas the infrared EDMs require a transmitter at one end and a reflecting prism at the other end. The recently-developed EDMs can measure distances without using reflecting prisms. These EDMs employ a time pulsed infrared signal transmitted by a laser diode to permit direct acquisition of distances from the target by using the target surface itself as a reflector. On the current market, many TS instruments use the infrared EDM, and can switch between the reflector mode and the non-reflector mode.

The reflector TS has been applied by Bulut and Tüdes [18] for measuring the trace length of fractures. In this study, the non-reflector TS was used for two purposes: i) for capturing the co-ordinates of a number of target points to quantify the fracture geometry; ii) for conducting the control surveying for registration of the target points, obtained by the close range digital photogrammetry and the laser radar methods.

2.2 Accuracy of the TS

Since the TS is an integrated instrument containing an EDM and an ET, the accuracy of measurements from the TS depends upon both the EDM and the ET. For a typical ET, the resolution can be up to 1″ (second of arc), and the accuracy is ranging from 0.5″ to 20″ for both horizontal and vertical angular measurements [23]. The resolution of an EDM can be up to 1 mm. The EDM's accuracy is usually quoted in the form of a mm ± b ppm (ppm = km^{-1}). The constant a is the instrument-dependent error, which is beyond the control of the users. It consists of the errors caused by the factors such as the unwanted phase shifts in electronic components, errors in phase measurement and index errors in centring the instrument. The varied quantity b is the systematic error, which is proportional to the distance being measured, and also depending on the atmospheric conditions at the time of measurement and on the frequency drift in the crystals of the modulation oscillator. The accuracy can be 5 mm ± 5 ppm for the EDM with standard infrared sources, and 5 mm ± 1 ppm for the EDM with laser sources [24]. But, different types of TS instruments have different technical specifications for the EDM's accuracy, ranging from 1 mm ± 1 ppm to 10 mm ± 10 ppm. Two types of the non-reflector TS have been used in this study. One is Leica TCRM 1102, which has the resolution of 1″ and the accuracy of 2″ for the ET, and its EDM has the resolution of 1 mm and the accuracy of 3

mm ± 2 ppm [25]. The other is Geodimeter 468DR, which has the resolution of 1″ and the accuracy of 2″ for the ET, and its EDM has the resolution of 1 mm and the accuracy of 5 mm ± 5 ppm [26].

In addition, when using the TS for fracture mapping, the co-ordinates of target points are used as the raw data for computing the geometrical parameters of fractures. So, it is important to notice how accurate the co-ordinates of a target point can be measured by the TS. However if just reading the information from the manual of a TS instrument, it is not clear enough for the geologists and geotechnical engineers to understand the accuracy of the TS measurements due to two main reasons: i) the manual only presents the resolution and accuracy of the distance measurements by the EDM and the angular measurements by the ET, respectively. No direct information about the co-ordinate measurements because it depends on the distance and angular measurements and difficult to provide a certain values; ii) the presented accuracy data in the manual is usually obtained in the standard mapping conditions, such as the emitted light or laser beam is almost perpendicular to the target surface, and the target surface is not rough but almost flat. But when measuring a target point on the rock faces, the mapping conditions are quite complicated. The accuracy of the target measurements might be affected by several influential factors, e.g. roughness of the fracture surface, inclination angle from the emitted light onto the rock faces. Therefore, the errors can be originated from two main sources: i) instrument-related errors; and ii) surface-related errors.

To provide a clear idea about the accuracy of the TS measurements, the error analysis theory was applied to estimate the accuracy of the point co-ordinates from the measurements of the EDM and the ET. A special test was conducted in this study to investigate the influence of the rock faces and fracture surfaces on the TS measurements. Since the co-ordinates of a target point are computed from the equation (1), the propagated errors (*dE*) of a point co-ordinates P(X, Y, Z) can be derived as follows [27]:

$$dE = \begin{bmatrix} dX \\ dY \\ dZ \end{bmatrix} = \begin{bmatrix} \frac{\partial X}{\partial S} & \frac{\partial X}{\partial \theta_V} & \frac{\partial X}{\partial \theta_H} \\ \frac{\partial Y}{\partial S} & \frac{\partial Y}{\partial \theta_V} & \frac{\partial Y}{\partial \theta_H} \\ \frac{\partial Z}{\partial S} & \frac{\partial Z}{\partial \theta_V} & \frac{\partial Z}{\partial \theta_H} \end{bmatrix} \begin{bmatrix} \varepsilon_S \\ \varepsilon_{\theta_V} \\ \varepsilon_{\theta_H} \end{bmatrix} = \begin{bmatrix} \frac{\partial X}{\partial S}\varepsilon_S + \frac{\partial X}{\partial \theta_V}\varepsilon_{\theta_V} + \frac{\partial X}{\partial \theta_H}\varepsilon_{\theta_H} \\ \frac{\partial Y}{\partial S}\varepsilon_S + \frac{\partial Y}{\partial \theta_V}\varepsilon_{\theta_V} + \frac{\partial Y}{\partial \theta_H}\varepsilon_{\theta_H} \\ \frac{\partial Z}{\partial S}\varepsilon_S + \frac{\partial Z}{\partial \theta_V}\varepsilon_{\theta_V} + \frac{\partial Z}{\partial \theta_H}\varepsilon_{\theta_H} \end{bmatrix} \quad (2)$$

Therefore,

$$dX = \frac{\partial X}{\partial S}\varepsilon_S + \frac{\partial X}{\partial \theta_V}\varepsilon_{\theta_V} + \frac{\partial X}{\partial \theta_H}\varepsilon_{\theta_H} \quad (3)$$

$$dY = \frac{\partial Y}{\partial S}\varepsilon_S + \frac{\partial Y}{\partial \theta_V}\varepsilon_{\theta_V} + \frac{\partial Y}{\partial \theta_H}\varepsilon_{\theta_H} \quad (4)$$

$$dZ = \frac{\partial Z}{\partial S}\varepsilon_S + \frac{\partial Z}{\partial \theta_V}\varepsilon_{\theta_V} + \frac{\partial Z}{\partial \theta_H}\varepsilon_{\theta_H} \quad (5)$$

where S is slope distance, θ_V is the vertical angle, θ_H is the horizontal angle; the errors of the co-ordinates of a point P(X, Y, Z) are dX, dY, dZ; ε_S, ε_{θ_V}, ε_{θ_H} are errors of the slope distance measurements from the EDM, and the vertical and horizontal angle measurements from the ET, respectively. The partial derivatives in equation (2) can be determined by:

$$\frac{\partial X}{\partial S} = \cos\theta_V \sin\theta_H, \quad \frac{\partial X}{\partial \theta_V} = -S\sin\theta_V \sin\theta_H, \quad \frac{\partial X}{\partial \theta_H} = S\cos\theta_V \cos\theta_H;$$

$$\frac{\partial Y}{\partial S} = \cos\theta_V \cos\theta_H, \quad \frac{\partial Y}{\partial \theta_V} = -S\sin\theta_V \sin\theta_H, \quad \frac{\partial Y}{\partial \theta_H} = -S\cos\theta_V \sin\theta_H;$$

$$\frac{\partial Z}{\partial S} = \sin\theta_V, \quad \frac{\partial Z}{\partial \theta_V} = S\cos\theta_V, \quad \frac{\partial Z}{\partial \theta_H} = 0$$

The above equations show how the accuracy of the point co-ordinates depends on the accuracy of both distance and angle measurements.

When measuring the target points on a fracture surface, some factors such as roughness of the surface, reflectance of the surface, inclination angle from the laser beam to the surface, also influence the accuracy of the point co-ordinates. These errors are of especial concern when measuring the targets on rock surfaces, and are called surface-related errors in this paper. To check the influence of the surface-related errors, a test study was performed. In this test, four factors are considered: i) inclination angle, i.e. the angle between the laser beam and the surface; ii) roughness of the surface; iii) reflectance of the surface; and iv) distance from the TS location to the targets.

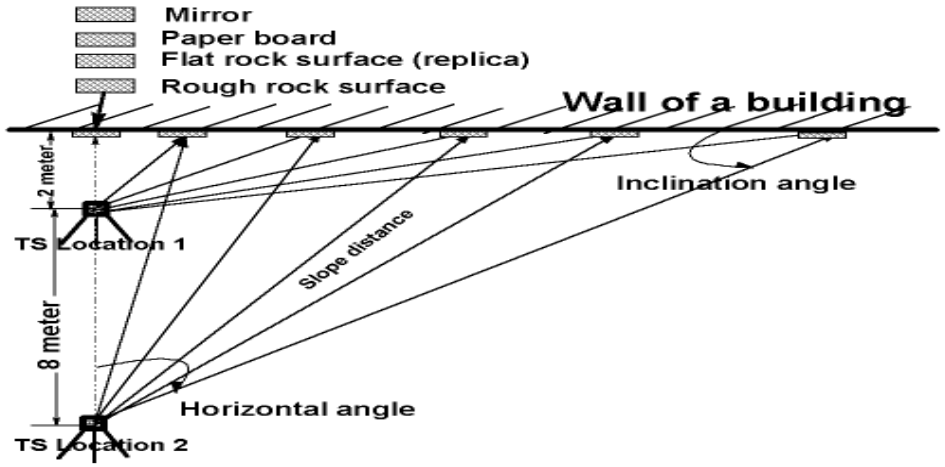

Figure 8. Accuracy test for the surface-related influential factors

Figure 8 schematically shows the test procedure. A vertical wall of a building, facing to the true North, was selected as a base plane. A non-reflector TS (Leica TCRM 1102) was standing at two locations (see Fig. 8) with a normal distance to the wall of about 2 m and 8 m, respectively. Small samples of four types of material surfaces are chosen: i) a mirror

surface; ii) a paperboard surface; iii) a silicon rubber replica surface of a flat fracture surface; iv) a sample of a rough fracture surface. These samples represent the fracture surfaces with different roughness and reflectance properties, and were put at different positions on the base plane. By the guidance of the ET, these samples were positioned along an almost horizontal band on the base plane. By adjusting the ET to make the vertical and the horizontal angle as zero degree, the laser beam was shooting perpendicularly onto the sample surface. Then, the horizontal angle was increased in order to decrease the inclination angle while keeping the vertical angle at zero degree. The surface-related errors can be detected by placing the samples in different positions along the wall. On each sample surface, a 8 cm segment was marked and pre-measured by a ruler with the accuracy of 0.5 mm, and then measured by the TS. Once the co-ordinates of the two end points of the segment were recorded by the TS, the length of the segment was calculated and compared with the length measured by the ruler.

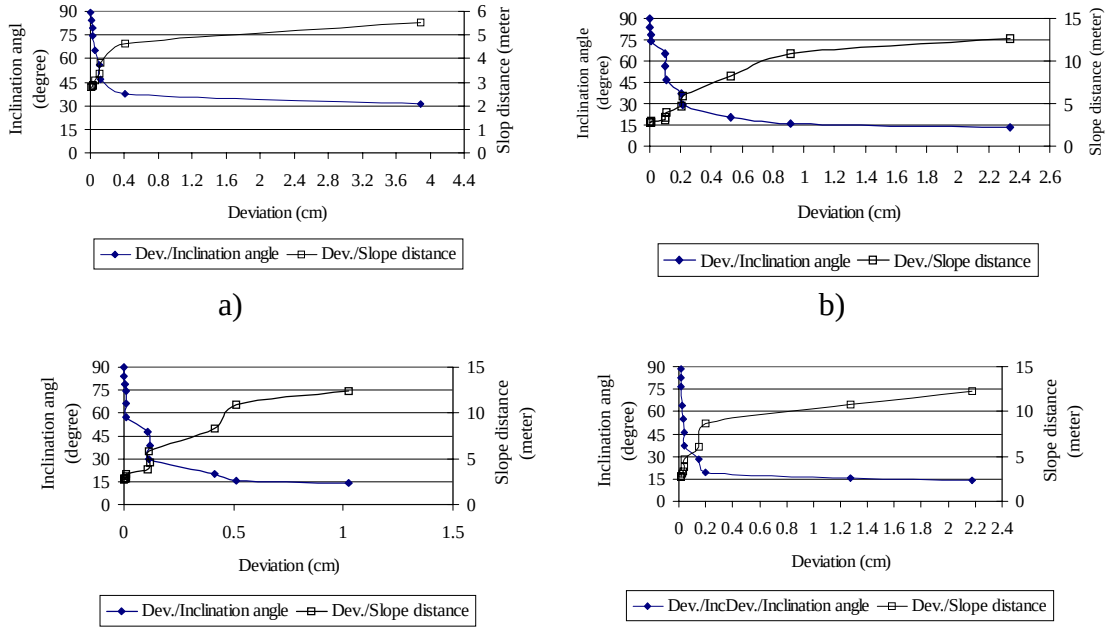

Figure 9. Test results for TS Location 1: the vertical distance = 2 m. a) a mirror surface; b) a paperboard surface; c) a replica surface; d) a rock surface.

Figure 9 and 10 show that the deviation (the X-axis) between the known length of the segment and the one measured by the TS is changed with the inclination angle (the left-side Y-axis) and the slope distance (the right-side Y-axis). The results indicate that the deviation is affected by the four influential factors. With decreasing inclination angles, the deviation is increased. Meanwhile, the deviation increases when increasing the slope distance. A threshold of inclination angle seems to exist for different surface conditions (see Table 1). If inclination angle is less than the threshold, the deviation is not acceptable. For the natural rock surface, the threshold is less than other surfaces, which indicated that the TS can measure a target point on the rock face with smaller inclination angle. But the roughness of the rock surface can affect the measurement of the targets.

The rougher the surface the bigger the deviation. Therefore, the surface-related errors must be considered when measuring targets on the rock faces by the TS.

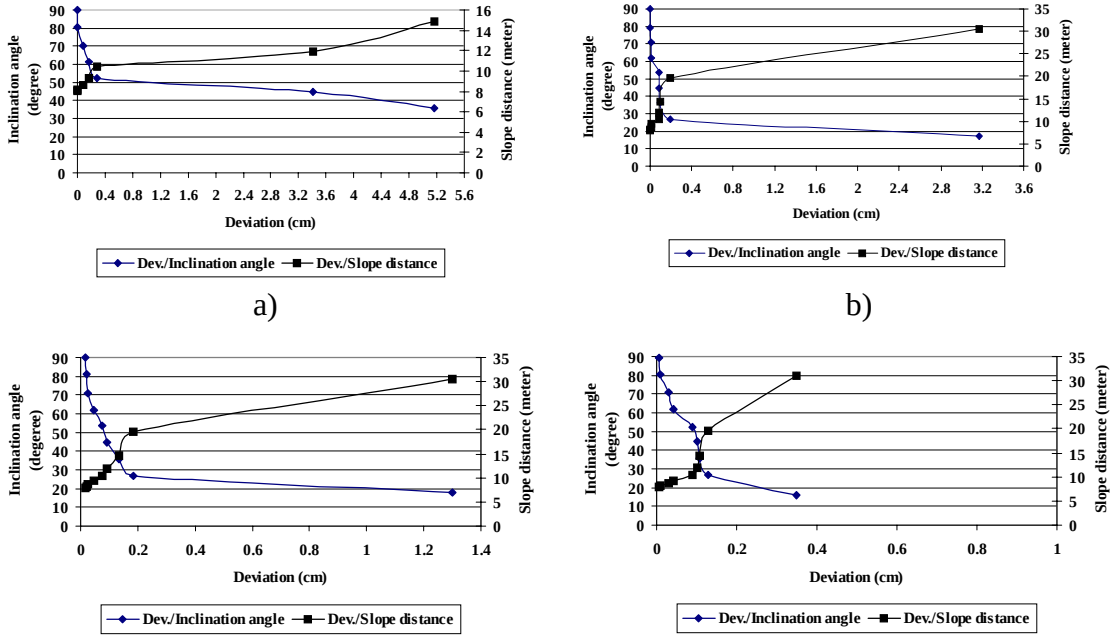

Figure 10. Test results for TS Location 2: the vertical distance = 8 m. a) a mirror surface; b) a paperboard surface; c) a replica surface; d) a rock surface.

Table 1. Threshold values of inclination angle of different surfaces

Material surface & Position of TS	Mirror		Paperboard		Replica		Rock	
	ε_{IA}	Dev	ε_{IA}	Dev	ε_{IA}	Dev	ε_{IA}	Dev
Location 1	37.8	< 4	28.9	<2	20.4	<4	19.5	<2
Location 2	52.5	<3	26.6	<2	26.5	<2	26.9	<2

Note: ε_{IA} = threshold of inclination angle (unit = degree), Dev = deviation between the known length and the length measured by TS (unit = mm).

2.3 Measuring fracture geometry

The key step for 3D mapping of fracture geometry is to capture the co-ordinates of a number of target points from the rock faces. To measure fracture geometry by the TS, three main steps must be taken as the following:

Step 1. Establishing a reference co-ordinate system

To capture the co-ordinates of target points by the TS, a 3D Cartesian co-ordinate system must be established. By using the TS, a local Cartesian co-ordinate system can be easily established in front of any rock faces in space. Since the true North needs to know for determining the orientation parameters of fractures, a geological compass or similar tools

must be used to help the TS to set up a co-ordinate system with the known true North (see Figure 7).

If necessary to link the local co-ordinate system to another local co-ordinate system or a known co-ordinate system in space (e.g. the national co-ordinate system and the geographical co-ordinate system), a number of control points (which have the known co-ordinates in a known reference space) must be found around the rock faces, or GPS (Global Positioning System) must be used.

Step 2. Sampling a number of target points to define fracture geometry

To quantify the geometrical parameters of fractures, a number of target points need to be sampled by the TS. The target points can be sampled either semi-automatically or fully automatically. The semi-automatic operation permits the user to select the targets on the rock face, and operate the TS to conduct the whole procedure of aiming and measuring the targets, and then storing the measurements. Meanwhile, by using a specially developed software, e.g. GeoPad [28] and TMS PROscan [29], the sampling procedure can also be automatically controlled.

When measuring the parameters of fracture geometry like spacing and trace length, it is better to capture the target points semi-automatically. To determine the orientation parameters of fracture planes, the targets can be either semi-automatically or fully automatically measured from the exposed fracture surfaces. To quantify the fracture roughness, it is necessary to control the TS to scan the fracture surface automatically in order to obtain the unbiased and regular sampled data. In this case, the TS is actually used as a point-sensing laser scanner.

Step 3. Computing fracture parameters from the recorded co-ordinates of points

Once the target points are captured by the TS, spacing and trace length of fractures are easy to be determined because these two parameters are actually the length of a segment or several segments.

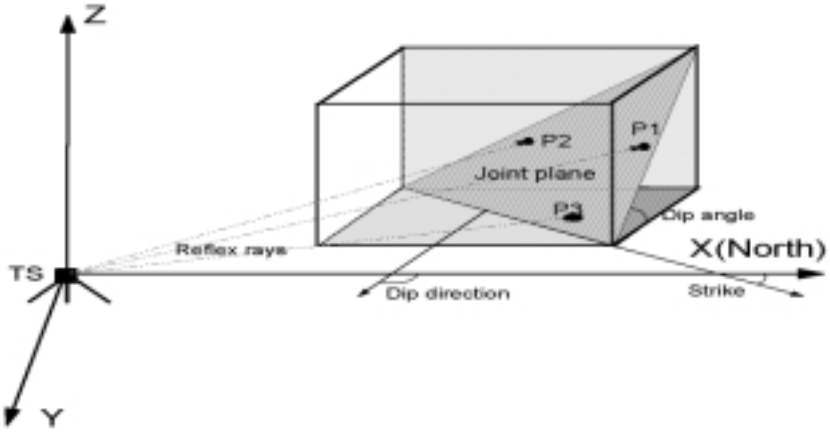

Figure 11. Determination of fracture orientation in a reference co-ordinate system

To quantify the orientation of fractures, the fracture planes have to be determined and the true north in the established co-ordinate system has to be known. Figure 11 schematically shows how to determine the orientation parameters of a fracture plane. An algorithm was developed in this study (Paper D) to compute the dip direction, dip angle and strike of a fracture plane, which will be summarised in Chapter 5.

The roughness of a fracture surface can also be quantified by the TS directly from the rock face with different sizes of samples and sampling intervals (Paper E). Figure 12 shows the scanning principle of a TS. By using the TS and a control program, e.g. Leica TMS PROscan, a target area on a fracture surface can be firstly defined by four corner points, e.g. P1, P2, P3 and P4 (or K1-K4 in the smaller window). The interval along the X-direction (P1-P2) and the Y-direction (P1-P3) can be set up with different values, with the minimum distance of 1 mm, respectively. Both an area and a scan-line on the fracture surface can be automatically scanned.

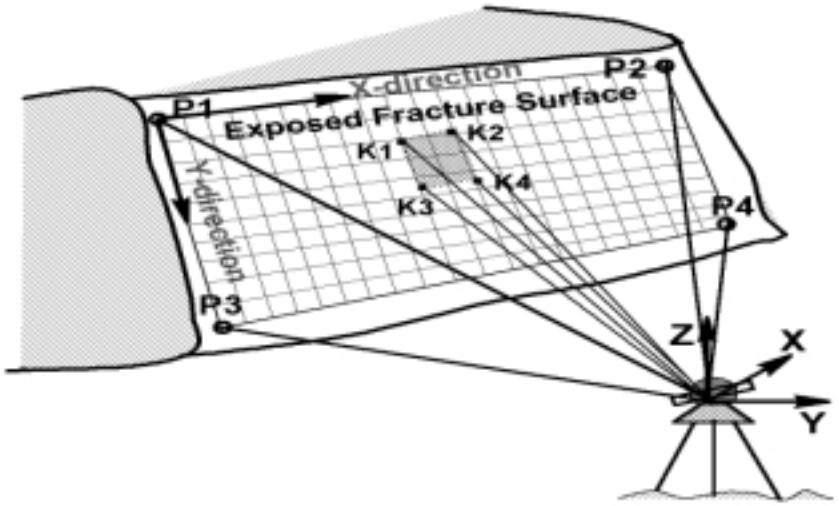

Figure 12. Automatic scanning of a fracture surface by a non-reflector TS

After selecting the target area and the point interval, the TS will automatically scan the fracture surface, point by point, along each scan-line. During the scanning, the position of the scanned points is continuously computed by the scanning program in the following ways:

i) Number of scan lines = $\frac{(\text{Distance of } (P1 - P3) + \text{Distance of } (P2 - P4))/2}{Y - \text{direction interval}}$;

ii) For each scan-line, the points are dispersed in a way, so that the defined interval in the X-direction is achieved as good as possible.

The scanning data are stored dynamically in a memory card inside the TS, and later downloaded to a PC for processing. Several methods, e.g. the variogram method [30], the spectral method [31], the structure function method [32] and the rough length method

[33], have been reported in the literature to be used for quantifying and characterising the roughness of a fracture surface.

Due to the resolution of the TS, the detailed roughness of a fracture surface is difficult to be detected by the TS method when comparing the measurements of the TS with those measured by a high resolution laser scanner. Thus, the presented method is particularly useful for in-situ measuring of the primary roughness or waviness of fracture surfaces.

2.4 Case study

In order to verify the TS method for fracture mapping at the rock faces, the case study has been conducted at three rock faces in Stockholm. For in-situ measuring of fracture geometry by the TS method, a portable mapping system was designed as shown in Figure 13, consisting of hardware and software.

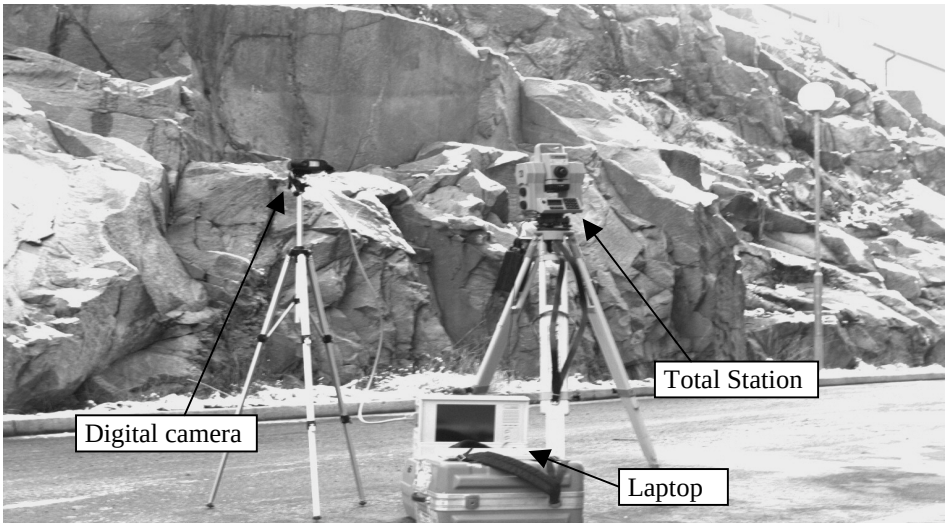

Figure 13. The on-site mapping system based on Total Station method

The hardware includes:
(i) a non-reflector total station (e.g. Geodimeter 468DR, Leica TCRM). This type of TS is used to capture co-ordinates of target points without touching the rock faces physically;
(ii) a digital camera (e.g. Kodak DCS200). The digital camera is actually optional in measuring fracture orientation using a TS. One can use the digital camera to record some additional mapping information (e.g. position of a scanline on the rock faces, fractures exposed on the rock faces and the distribution of captured points on the fracture surface) for posterior analysis of the mapping data.
(iii) a portable computer which is used to download the data from the TS and the digital images of the rock faces from the digital camera to a PC. Calculation of fracture orientation and analysis of the fracture networks in the rock mass can be done immediately in the field.
(iv) some accessories are also needed, such as a compass, cables, tripods etc.

The software consists of:
(i) programs to control the TS, which are usually provided by the TS manufacturer;
(ii) programs to download the co-ordinates of points from the TS to the PC;
(iii) programs to download and edit images taken by the digital camera;
(iv) programs to calculate fracture orientation;
(v) programs to analyse the fracture network or for any rock engineering applications.

To measure the orientation of fracture surfaces, a number of target points are semi-automatically captured by the non-reflector TS. The amount of the target points captured from each fracture surface depends on how rough or wavy the surfaces are. The rougher the surface is, the more the points must be captured. In addition, The exposed patterns of fractures on the rock face can be divided into three types as shown in Figure 14. The way in which a best-fit plane approximating the fracture surface can be defined depends upon the exposure pattern of fractures. In case 1, the fracture surface is partly exposed as a facet with a certain area. A number of non-collinear points can be selected on the facet to define the fracture plane. In case 2, the fracture surface is exposed as two or more non-collinear trace lines instead of a facet. In this case, a number of non-collinear points can be selected along the relief trace lines of the fracture surface. Then the fracture plane can be defined. In case 3, the fracture surface is exposed as a straight line on the rock surface. In this case, non-collinear points can not be found along the straight line and the best-fit plane of the fracture surface can not be defined. Therefore, only if the fractures are exposed as in the first two cases, can the fracture orientation be determined by using the TS method or any other methods.

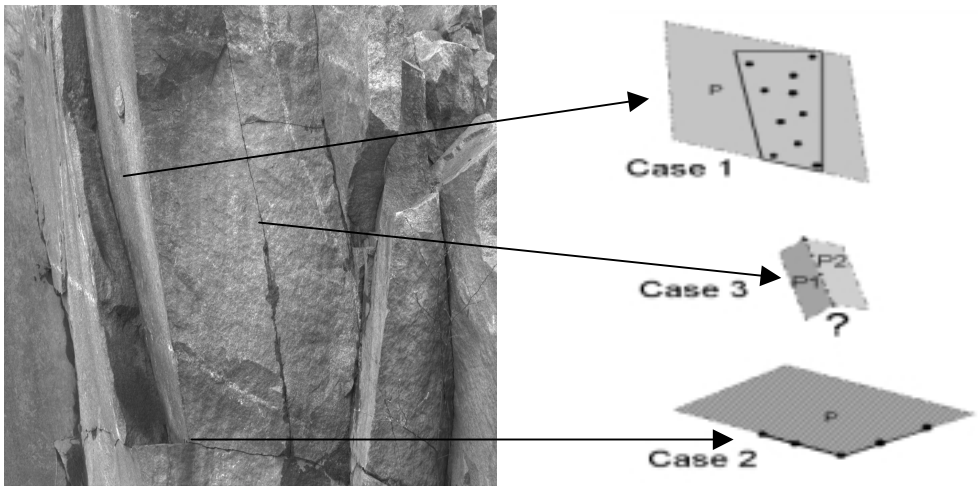

Figure 14. Three cases of definition of discontinuity exposures at rock faces

Orientation measurements of some fractures exposed on the rock faces are listed in Table 2. All the fractures in case 1 listed in Table 2 have an exposed surface with an area larger than 10 cm x 10 cm. The exposed surfaces of these fractures are not too rough. Target points on each fracture are distributed as far as possible from each other. When measuring fracture orientation by using a compass-inclinometer, the measurements are

carefully performed in order to get correct data to compare to the measurements made by the TS method.

Results shown in Table 2 indicate that the deviation between the TS method and the compass-inclinometer method for the dip angle has a range of 1 - 7 degrees with an average of 2.4 degrees. The deviation for dip direction is 4.8 degrees on average, with a range of 1 - 9 degrees. This deviation of the measurements is acceptable for the most of rock engineering applications.

The case study indicated that several factors might affect the accuracy of fracture orientation measurements, such as exposure pattern of fracture surfaces, roughness of the fracture surfaces, exposed size of the fracture surface, point distribution on the fracture surface, the amount of points captured from each fracture surface, measurement accuracy of the true north by using the compass when setting up the local Cartesian co-ordinate system. These factors must be taken into consideration when the TS method is used to measure the fracture orientation.

A case study was performed at a road-cut rock face for measuring the undulation of a larger fracture surface in order to validate the applicability of the TS method. The rock face is located along highway E4 in the north-western Stockholm. The fracture is cutting through a greyish-red, medium-grained granite rock and belongs to a NW-SE extensional fracture zone. The fracture surface exposed at the rock face is about 20 m × 15 m. A part of this larger fracture surface (about 9 m × 2.5 m) and a small window inside this part (about 20 cm × 20 cm) were scanned by the TS method (see Figure 15).

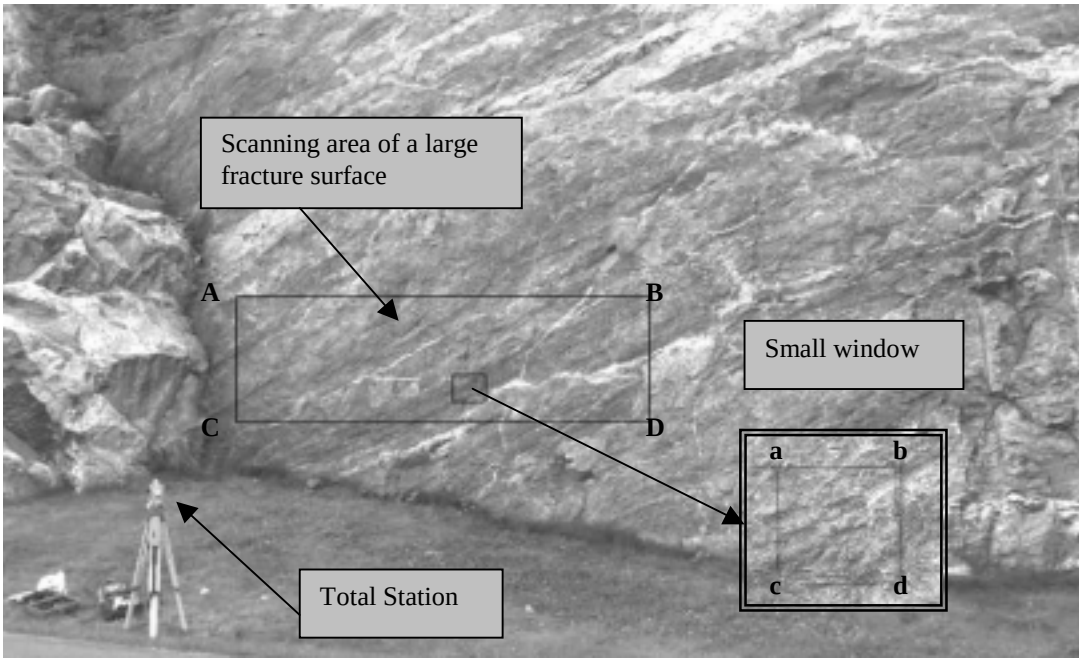

Figure 15. In-situ scanning of a large fracture surface by the non-reflector TS

Table 2 Test results of discontinuity mapping at the exposed rock faces

F-No	Exposure case	Manual		Total Station			Deviation	
		DD	DA	DD	DA	Pn	Δ|DD|	Δ|DA|
F1	Case 1	20°	66°	16°	68°	4	4°	2°
F2	Case 1	291°	80°	294°	75°	4	3°	5°
F3	Case 1	301°	72°	299°	71°	6	2°	1°
F4	Case 2	230°	28°	237°	32°	3	7°	4°
F5	Case 1	306°	83°	315°	80°	4	9°	3°
F6	Case 1	308°	89°	310°	88°	5	2°	1°
F8	Case 1	282°	87°	281°	86°	8	1°	1°
F9	Case 1	141°	42°	137°	38°	4	4°	4°
F10	Case 1	26°	86°	31°	85°	4	5°	1°
F12	Case 1	323°	88°	315°	89°	4	8°	1°
F13	Case 1	332°	90°	325°	89°	4	7°	1°
F14	Case 1	324°	90°	318°	89°	4	6°	1°
F15	Case 1	10°	68°	9°	66°	5	1°	2°
F16	Case 1	327°	27°	335°	31°	3	8°	4°
F17	Case 1	238°	84°	240°	83°	5	2°	1°
F18	Case 2	205°	14°	198°	21°	3	7°	7°
F19	Case 2	326°	25°	327°	28°	5	1°	3°
F20	Case 1	282°	87°	281°	86°	8	1°	1°
F21	Case 1	141°	46°	135°	49°	4	6°	3°
F22	Case 1	9°	56°	16°	59°	4	7°	3°
F23	Case 1	323°	88°	317°	87°	4	6°	1°
F24	Case 1	26°	87°	32°	86°	3	6°	1°
F25	Case 1	324°	90°	327°	89°	5	3°	1°
F26	Case 1	10°	68°	14°	67°	4	4°	1°
F27	Case 1	327°	27°	332°	32°	3	5°	5°
F28	Case 1	238°	84°	240°	83°	6	2°	1°
FP1	Case 1	46°	80°	52°	85°	12	6°	5°
FP2	Case 1	300°	75°	305°	72°	8	5°	3°
FP3	Case 1	28°	60°	33°	61°	5	5°	1°
FP4	Case 1	318°	86°	324°	83°	5	6°	3°
FP5	Case 1	308°	87°	313°	88°	5	5°	1°
FP6	Case 1	140°	85°	146°	83°	5	6°	2°
FP7	Case 1	318°	87°	324°	84°	6	6°	3°
FD1	Case 1	59°	84°	63°	86°	5	4°	2°
FD2	Case 1	210°	73°	214°	72°	4	4°	1°
FD3	Case 1	215°	86°	221°	79°	3	6°	7°
FD4	Case 1	292°	87°	301°	88°	4	9°	1°
				Average deviation			4.8°	2.4°

(Note: DD = Dip Direction, DA = Dip Angle, Δ|DD| = absolute value for deviation of dip direction between manual method and TS method, Δ|DA| = absolute value for deviation of dip angle between traditional manual method and TS method, Pn = number of recording points)

A non-reflector TS, Leica TCRM1102, and the scanning program, Leica TMS PROscan [29], were used for scanning the fracture surface. The TS was positioned at a distance of about 7 m away from the rock face. Before scanning, an oriented local Cartesian co-ordinate system with the known true north was established by using the TS and a compass. The orientation of the fracture surface and the directional features of the fracture roughness in space can be analysed. Four corner points, *A*, *B*, *C* and *D*, were sequentially measured to define the scanning area with the size of 9 m × 2.5 m. The sampling interval along the X-direction (e.g. *A*-*B*) and the Y-direction (e.g. *A*-*C*) was then defined as 10 cm interval for both directions. A small window of 20 cm × 20 cm inside this area was selected to be scanned at 5 mm interval in order to study the scale effect on fracture roughness. The scanning data were first stored in a PCMCIA Flesh memory card in the field, and later downloaded to the PC for data processing. The software Surfacer Imageware [61] was used for roughness analysis.

To analyse the roughness of the large scanning area, a rectangular area of 8 m × 2 m was selected. The fractal parameters of the selected surface were calculated by using the RL method. In this case, a series of sampling windows with the size *w* of 400, 500, 1000 and 2000 mm were chosen. The standard deviations of reduced asperity height *S(w)* were computed for the series of window sizes *w*, and plotted in a log-log diagram (see Figure 16a). A very good linear relationship was obtained. The roughness of the large surface can be characterised by D = 2.2517 and A = 0.0493.

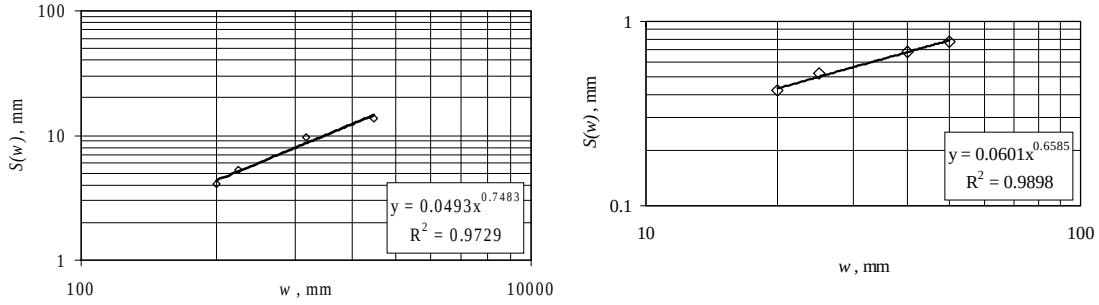

(a) (b)

Figure 16. Standard deviation of reduced asperity height S(w) versus window size w for the large rectangular surface (a) and the small window surface (b) of the large fracture.

Using the same analysis method, the roughness of the small window inside the scanned surface was quantified. Within the area of 200 mm × 200 mm, a series of square sampling windows with the defined size *w* of 20, 25, 40 and 50 mm were chosen. Figure 16b shows the relationship for the standard deviations of reduced asperity height *S(w)* versus the window size *w*. The fractal parameters of the small window are estimated as *D* = 2.3415 and *A* = 0.0601. The results indicate the existence of a scale effect for the large surface and the small window. The discrepancy is due to different density of sampling points, different position on the fracture surface, and different sizes of the sampling windows.

2.5 Conducting the control surveying

The TS can also be used for control surveying if other methods, e.g. photogrammetry and laser scanner, are applied for fracture mapping. The purpose of the control surveying is: i) transformation of the target points between different co-ordinate systems, e.g. from the image or laser scanner co-ordinate system to the TS co-ordinate system; ii) registration of different parts of the rock face all together in order to create an integral 3D model of the rock face.

There are two cases for control surveying at the rock faces: i) there are some known points (their co-ordinates are known within a co-ordinate system) around the rock faces; ii) no known points can be found near the rock faces. In the former case, the known points are used to resect the position of the TS instrument, and then all the points captured in the TS co-ordinate system are transformed into the known co-ordinate system, e.g. the national ground co-ordinate system or the global geographical co-ordinate system. In the latter case, the TS is first used to establish a local co-ordinate system in one (if the rock face is small so that all target points are within the covering range of the TS) or several positions (if the rock face is too large or varied on the surface to be covered by locating the TS in one position), and then all points measured by the TS in different positions are linked together. If GPS (Global Positioning System) is used, the position of the TS instrument in space can be measured, and then the local co-ordinate system established by the TS can be linked to the global co-ordinate system.

To register different parts of the rock face together and transform the target points between different co-ordinate systems, at least three control points need to be measured, and these control points must be seen in both parts. The control points have to be marked on the rock face by some way, or some identifiable points on the rock face are selected as the control points.

2.6 Pros and cons of the TS method

Results of this study indicate some pros and cons of the TS method for fracture mapping. The pros of this method are:

1) it can be independently used for fracture mapping because all mapping tasks, e.g. establishing the co-ordinate system, control surveying and capturing the co-ordinates of the target points, can be carried out by the TS;
2) it is easy to be operated by the user, no need for special training or background knowledge;
3) fracture mapping in a large distance without touching the rock face physically;
4) the target points can be actively captured according to the requirement of the users;
5) the captured data can be fully used for quantifying fracture geometry without recording any unused measurements;
6) it is portable so that suitable for in-situ fracture mapping.

Th cons of this method can be:

1) low sampling speed for capturing a large number of target points;
2) it can not record the visual information so that impossible for visual mapping;
3) different TS instruments have different operation commands so that not convenient for the users to use different types of TS instruments. But if an extra system, e.g. GeoPad [28], is used, several types of the TS instruments can be operated with the same commands and software.

3. Close-range digital photogrammetry method

Photogrammetry is a technique for three-dimensional mapping of objects from images or photos based on the principle of triangulation. By taking photos or images from at least two different positions and measuring the corresponding image points of the same target points in each image, the light rays of target points of an object can be numerically reconstructed and intersected from the two (or more) corresponding image points. By triangulation, 3-D co-ordinates of the targets may be calculated in a reference object co-ordinate system. Depending on different applications, photogrammetry can be categorized in two groups: 1) aerial photogrammetry for generation of topographic maps; and 2) close-range photogrammetry for measurement of terrestrial objects typically with the extent of less than about 100 meters. If digital images of the objects are used, instead of hard copy photos, the mapping techniques can be termed as digital photogrammetry. Close-range photogrammetry techniques have already been applied in many disciplines, such as architecture, archaeology and medicine. According to the ways for acquisition of the images and restitution of the target points, photogrammetry can also be divided into stereo photogrammetry and convergent photogrammetry. Reviewing the former work of rock engineering applications, stereo photogrammetry have been used for characterizing fracture geometry [7, 11, 12, 13] and for investigating rock mass deformation [34]. In this study, convergent restitution techniques of photogrammetry were applied for measurement of fracture geometry, and a non-reflector total station was used for control surveying. This method is described in Paper B. The principles of this method and results of the case study are briefly presented in this Chapter.

3.1 Principle of photogrammetry and two types of restitution techniques

The fundamental geometrical principle of photogrammetry is the central perspective. According to this geometrical law, photogrammetric restitution is just an inverse procedure of photographing. Photography creates the image by projecting the 3-D object onto the 2-D projective planes, while photogrammetric restitution aims to reconstruct the 3-D object from several (more than two) 2-D images to a 3-D reference space. Figure 17 shows schematically the principle of the central perspective. An object point, *A* (X_A, Y_A, Z_A), in an object space is projected onto the projective plane by a straight line, *A-O-a*, from the object point *A* passing through the perspective center *O* to the image point *a* (x_a, y_a). The perspective axis *P-O-p* is orthogonal to the projection plane and intersects the plane at *p*, the principal point. The distance *O-p* from the perspective center to the projective plane is the principal distance, usually denoted by *c*. The relationship between the object and image points *A* and *a* can be described by a three-dimensional transformation of a point between two Cartesian co-ordinate systems (Fig. 17). The primary co-ordinate system (X-Y-Z) is arbitrarily located in the object space. Within this co-ordinate system, the perspective center *O* and the object point *A* have the co-ordinates (X_0, Y_0, Z_0) and (X_A, Y_A, Z_A), respectively. The secondary co-ordinate system (x-y-z) has its origin at the perspective center *O*. The scale factor between these two systems is unity. The z-axis coincides with the camera principal axis and is directed away from the projective plane. The x- and y-axes are parallel to the projective plane and are directed so as to create a right-hand system. So, the 3-D co-ordinates of the point *a* in the secondary

co-ordinate system become (x_a, y_a, -c). Then, the relationship between *A* and *a* in vector form, i.e. $\mathbf{X_A}$ and $\mathbf{x_a}$, can be written as:

$$\mathbf{X_A} = \mathbf{X_O} + \mathbf{S} \tag{6}$$

where **S** is the position vector of *A* relative to *O*. **S** is collinear with $\mathbf{x_a}$, but with opposite direction. Therefore:

$$\mathbf{X_A} = \mathbf{X_O} - \mu\mathbf{R}^t\mathbf{x_a} \tag{7}$$

which in matrix notation is the collinearity equation:

$$\begin{bmatrix} X_A \\ Y_A \\ Z_A \end{bmatrix} = \begin{bmatrix} X_0 \\ Y_0 \\ Z_0 \end{bmatrix} - \mu \begin{bmatrix} r_{11} & r_{21} & r_{31} \\ r_{12} & r_{22} & r_{32} \\ r_{13} & r_{23} & r_{33} \end{bmatrix} \begin{bmatrix} x_a \\ y_a \\ -c \end{bmatrix} \tag{8}$$

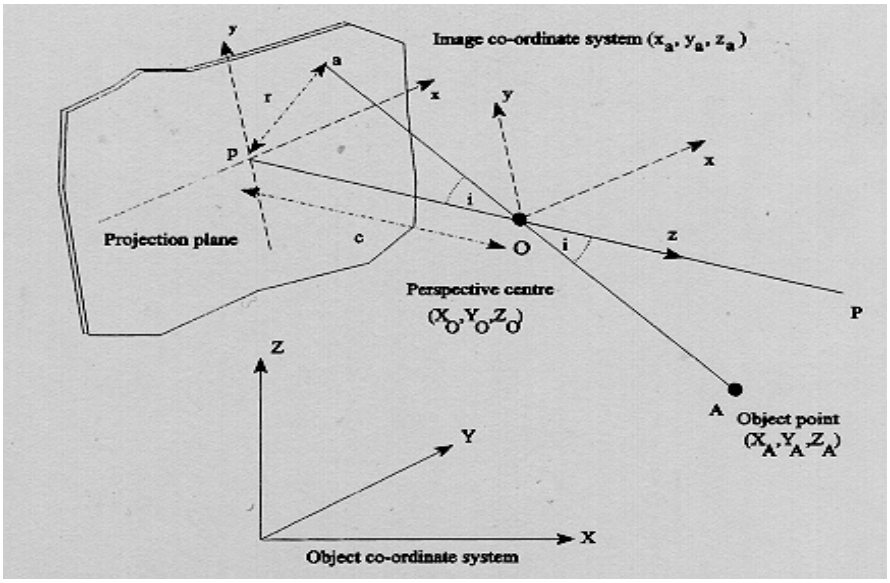

Figure 17. Central perspective projection (from Cooper & Robson [35])

In equations (7) and (8), μ is a scalar quantity greater than zero, and r_{ij} (i, j =1, 2, 3) are the elements of a rotation matrix *R* between the co-ordinate systems of X-Y-Z and x-y-z:

$$R = \begin{bmatrix} r_{11} & r_{12} & r_{13} \\ r_{21} & r_{22} & r_{23} \\ r_{31} & r_{32} & r_{33} \end{bmatrix} \tag{9}$$

where r_{ij} are the functions of ω, φ, κ. $r_{11} = \cos\varphi\cos\kappa$, $r_{12} = \sin\omega\sin\varphi\cos\kappa + \cos\omega\sin\kappa$
$r_{13} = -\cos\omega\sin\varphi\cos\kappa + \sin\omega\sin\kappa$, $r_{21} = -\cos\varphi\sin\kappa$, $r_{31} = \sin\varphi$, $r_{32} = -\sin\omega\cos\varphi$
$r_{22} = -\sin\omega\sin\varphi\sin\kappa - \cos\omega\cos\kappa$,
$r_{23} = \cos\omega\sin\varphi\cos\kappa + \sin\omega\cos\kappa$, $r_{33} = \cos\omega\cos\varphi$

ω is the rotation angle around x-axis, φ is the rotation angle around y-axis, κ is the rotation angle around z-axis.

Equations (6), (7) and (8) are the basis for photogrammetric restitution, which indicate that the object co-ordinates of a point in principle can be determined if its image co-ordinates are known. In addition, the data of the inner and outer orientation of the image, as well as the scale factor μ, are also needed. The position of the principal point *P* (or *PP*) and the principal distance *c* are termed as the elements of the inner orientation in photogrammetry. The object co-ordinates of the camera position (X_0, Y_0, Z_0) and the rotation angles (ω, φ, κ) of the image co-ordinate system are termed as the elements of the outer orientation in photogrammetry. The elements of the inner orientation can be obtained from the camera calibration specification. The elements of the outer orientation can be determined by surveying several control points, resulting in known co-ordinates of these points, both in a reference object co-ordinate system and in the image co-ordinate system.

The scalar quantity μ is unique for every ray (every object point vector), which is unknown. Therefore, to determine the position of a target point in space, at least two images of the same point are required. In photogrammetry, stereo and convergent restitution techniques are widely used. With stereo restitution, two images are taken with their camera axes, more or less, parallel to each other and perpendicular to the baseline (see Figure 18a). The base, i.e. the distance between the two camera perspective centers, is usually chosen so that the two images overlap by about 60 percent [36]. Then, photogrammetric restitution is carried out by using equipment or computers, providing stereoscopic perception of the object by, e.g. standard optical viewing with twin screens or split screen or an overlay with anaglyph, polarizing or synchronized shutter.

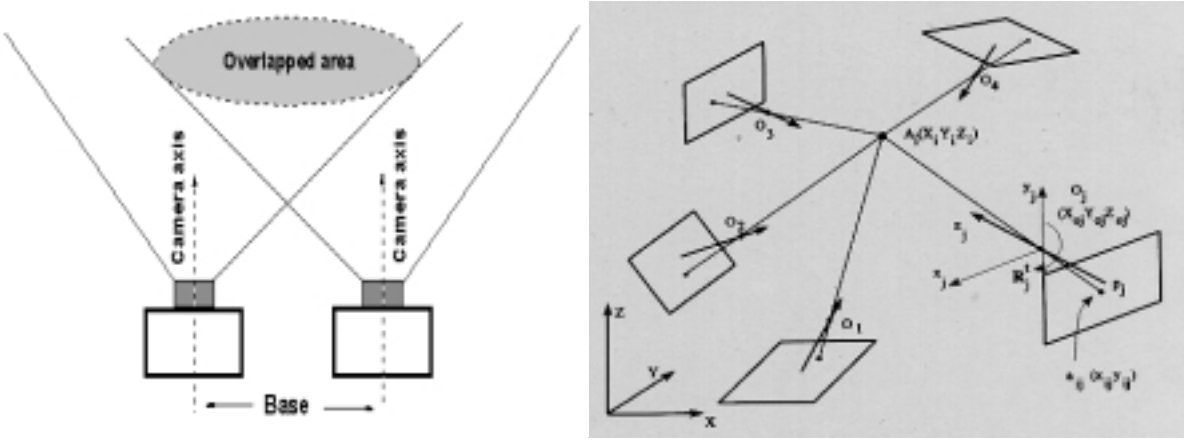

(a) (b)

Figure 18. Stereo photogrammetry (a) and convergent photogrammetry (b)

With convergent restitution (see Figure 18b), more than two images of a mapping area are taken convergently from different angles and distances. This means that stereoscopic impression of the object can not always be obtained. The target points are sequentially identified and measured in each image. Then, the object co-ordinates of the target points are determined by a multistation convergent bundle adjustment technique [35]. In the bundle adjustment, all measured image co-ordinates of the points are processed

simultaneously, using linearized collinear equations. The equation system is solved by least squares adjustment, resulting in exterior (and sometimes improved interior) orientation elements and object co-ordinates of the points.

The stereo photogrammetry method has been used for fracture mapping in the research work presented in [7, 11, 12, 13]. The target points are easily recognized by stereoscopic viewing of the image pairs, even if they are poorly defined. Convergent photogrammetry gives the operator more freedom of photographing the objects, which is convenient for fracture mapping at rock faces. If the target points are clearly identified, this method can provide high degree of reliability and accuracy of the measurements. In this study, the convergent photogrammetry was used for measuring fracture geometry from several images of the rock faces.

3.2 Procedure of fracture mapping by convergent photogrammetric techniques

Five steps must be taken for fracture mapping at rock faces by using the convergent photogrammetry method: i) camera calibration; ii) control surveying by a non-reflector total station; iii) taking images of the mapping scenes; iv) applying a close range photogrammetric software, i.e. PhotoModeler, for photogrammetric restitution of the target points; v) quantifying fracture geometry from the recorded co-ordinates of target points.

3.2.1 Camera calibration

Camera calibration aims at determining the optical and geometrical parameters of a camera that is going to be used for photographing the objects. The elements of interior orientation, i.e. x_a, y_a, and c, must be known in order to be able to reconstruct the outer bundle of rays. In addition, the optical image distortion of the camera lens must be known. For a metric camera, these parameters are given by the camera manufacturer. However, for a non-metric camera, a camera calibration must be performed.

In this study, a non-metric digital camera was used. Therefore, a test range calibration method was applied. A test field was developed by Torlegård [37]. In the test field, a number of accurately positioned targets are fixed in five planes within a 3-D steel frame. The test field was photographed from three different positions. A Kodak DCS200 digital camera with solid state CCD sensor and a 28 mm focal length lens was calibrated and used to take the images of the rock face. The sensor has a resolution of 1524 by 1012 pixels on a 14 mm by 9.3 mm chip. The target points were first measured on images displayed on the computer screen, and then the measured data were input to the calibration software to determine the camera calibration parameters. The parameters resulted from the camera calibration include the calibrated principal distance, the co-ordinates of the principal point *PP* (Xpp, Ypp), Figure 19a cf. Figure 17 (x_p, y_p) on the image plane, and the radial distortion. In the digital image, the principal point is defined in pixel co-ordinates (r, c) with the origin in row-1 and column-1, and then transformed into image co-ordinates (x, y), which has a temporary origin in the lower left-hand corner of the image (see Figure 19). The calibration results are shown in Figure 19a, b, which

indicates the lens suffers a certain radial distortion. These data are required as input parameters by the photogrammetric restitution software, in this case the PhotoModeler.

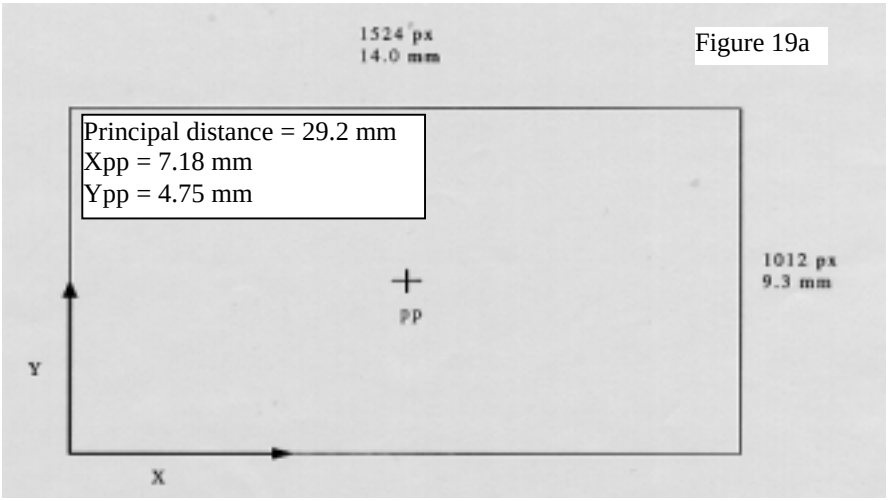

Figure 19a

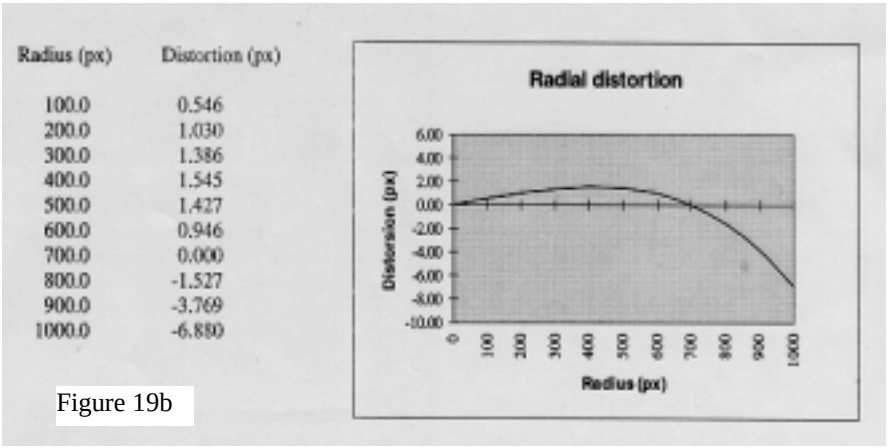

Figure 19b

Figure 19. Camera calibration results of the Kodak DCS200 digital camera with a 28 mm focal length lens: a) Co-ordinate system of camera CCD chip, b) Radial distortion.

3.2.2 Control survey

The objectives of control survey are: i) establishing a reference 3-D co-ordinate in object space; ii) determining object co-ordinates of a number of control points; iii) determining the elements of exterior orientation of the camera positions; iv) transforming the measured points from 2-D image co-ordinate systems to a 3-D object co-ordinate system.

Control surveying was usually done in the former work by using several known control points around the mapping area and connecting them to an existing co-ordinate system [13], or attaching several markers on the measured rock face and establishing a new local

co-ordinate system [7, 11, 34]. In this study, a non-reflector geodetic total station was applied for control survey.

Using the non-reflector TS, control points can be remotely measured without physically touching the rock face. Some clearly identifiable targets on the rock face can be selected as control points. The control points must be well distributed within the mapping area. At least four control points must be photographed in each image in order to guarantee the reliability and accuracy of the photogrammetric restitution. The data file of the control points, recorded by the TS, are then downloaded to the photogrammetric restitution software, PhotoModeler, for determining the position and attitude of the camera (termed as the elements of the outer orientation in photogrammetry) and transforming all target points from the image co-ordinate system to the established object co-ordinate system.

3.2.3 Taking images

The images of the rock face must be properly taken in order to be suitable for the photogrammetric restitution techniques. Since the multistation convergent bundle adjustment technique was used, a number of images (at least three) must be taken from different angles.

For each mapping area of the exposed rock face, the images are usually taken from the front, the right side and the left side (see Figure 20). The angles between each of two imaging rays from one and the same point in the object should be as close to 90 degrees as possible in order to minimize the intersection errors. However, too large angles give rise to other problems. Details are obstructed or difficult to be identified because of the topography of the rock face. The adjacent images must be overlapped as much as possible in order to capture as many features and targets as possible in the images. It is advantageous to capture more than three images, from different directions, for each mapping area in order to take redundant measurements and improve the measurement accuracy.

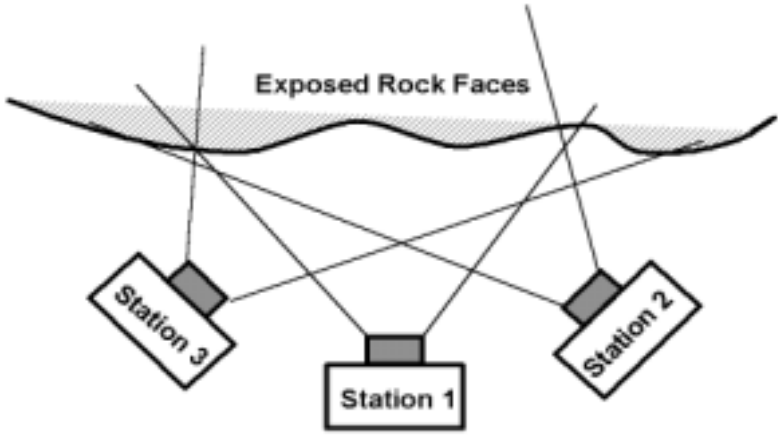

Figure 20. Arrangement of camera positions for a mapping area

3.2.4 Restitution of the target points

The close range photogrammetric software, PhotoModeler 3.1 [62], was used in this study to recover the positions of target points in space for 3-D fracture mapping. This software is developed on the basis of the multistation convergent bundle adjustment technique. It has been applied for 3-D mapping in different fields, such as architecture, archaeology, forensics and accident reconstruction. To obtain object co-ordinates of the targets by using PhotoModeler, five main steps are carried out:

Inputting calibrated parameters of the camera
When using PhotoModeler for photogrammetric restitution, the camera-lens combination needs to be described, such as focal length, image resolution, CCD chip size, image co-ordinates of the principal point and lens distortion. These parameters are obtained from the camera manufacturer and from the camera calibration.

Downloading the images and the co-ordinate data file of control points
PhotoModeler accepts images of the mapping object to be taken as either grey-level or colour images in different format, e.g. tiff, bmp, Gif, JPEG. The co-ordinates of control points, pre-captured by the non-reflector total station, must be downloaded and imported to PhotoModeler as DXF file, ASCII text CTL file or Cube shape file.

Marking control points and target points in each image
To determine the object co-ordinates of target points in 3-D space, the image co-ordinates of both control points and target points must be known. When using PhotoModeler for photogrammetric restitution, the operator has to sequentially identify and mark the control points and the target points in each image (see Figure 21). Marking of a point means measuring its position (row and column) in the digital image. The measured points in each image must be clearly identifiable. The control points (marked with triangles) need to be measured first, and then the target points (marked with crosses).

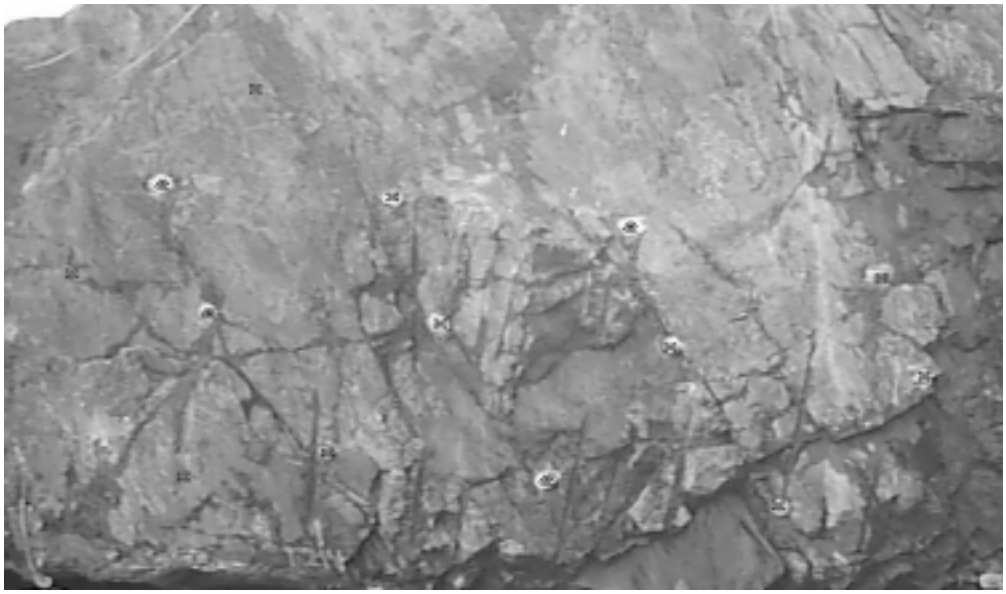

Figure 21. Marking control points (Δ) and target points (×) in image with PhotoModeler

Referencing the image points of the targets displayed in different images

One of the most fundamental processes for photogrammetric restitution is to identify and measure conjugate points in two or more overlapping images, which is termed as image matching in photogrammetry. The referencing functions in PhotoModeler enable the operator to perform image matching semi-automatically. After the image points of the targets are identified and marked in each image, PhotoModeler requires the operator to indicate whether a point in one image is the conjugate point in other images, which correspond to the same object point in 3-D space.

Determining the co-ordinates of the target points

Once all the data required for restitution are obtained by the above steps, PhotoModeler will automatically process those data to determine the co-ordinates of the target points in the established Cartesian co-ordinate system. However, data processing is not always successful due to the error propagation in the above steps. Errors may produce from control surveying, from too few images, and from marking and referencing. Therefore, the operator has to check and improve the operation in each step until the data processing becomes successful.

3.2.5 Quantification of fracture geometry

By combining non-reflector total station measurements and close range photogrammetric techniques, co-ordinates of target points on a rock face or any other objects can be successfully obtained. The geometrical parameters of fractures, e.g. trace length, spacing, dip angle and dip direction, can be readily computed from the recorded co-ordinates of the target points. The algorithms for determining these fracture parameters will be presented in Chapter 5.

3.3 Case study

In the case study, the presented method was applied for measuring the trace length, the dip angle and dip direction of fractures at two selected road-cutting rock outcrops in Stockholm.

For each mapping area, three or four of the captured images were used, and at least four control points were measured for determining the co-ordinates of target points. Two examples are shown in Figure 22. The control points were carefully chosen so that they are well distributed within the mapping area and clearly identified. The target points were also properly selected in order to be identifiable in each image. Features of the rock faces, such as edges, cracks, colour and surface texture, were used to recognize and identify the conjugate points in each image.

In order to check the mapping accuracy, we also used the total station method to quantify the geometry of these fractures. Parts of the mapping results and the comparison between

the presented method and the total station method are listed in Table 3. The maximum deviation between the two methods for dip direction (DD) is 10.5 degrees, and for dip angle (DA) 5.2 degrees. The measurement accuracy is affected by several factors, such as measurements of control points from the TS, camera calibration, number of control points and images used for photogrammetric restitution, convergent angle between the photographing directions, errors from marking and referencing of the conjugate points in each image, and especially the errors of identification of target points in each image.

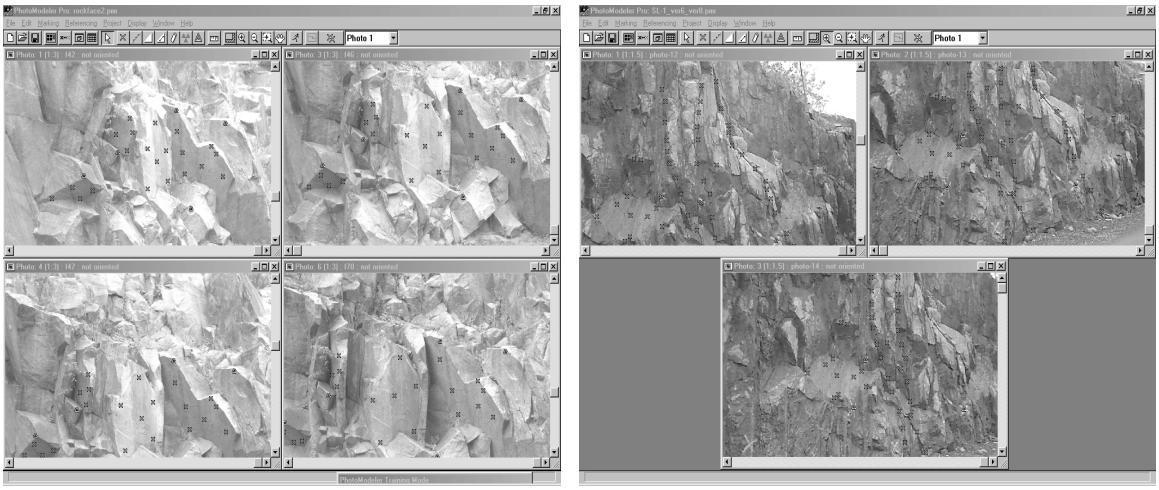

Figure 22. Determination of target points at two exposed rock faces by PhotoModeler

Table 3. Mapping results of case study at exposed rock faces

Geometry of fractures	CRDP method	TS method	Deviation
DD/DA of FN-1	18.5° / 76.4°	27.1° / 71. 2°	8.6° / 5.2°
DD/DA of FN-2	120.3° / 78.3°	124.2° / 74.5°	3.9° / 3.8°
DD/DA of FN-3	104.1° / 81.2°	98.3° / 78.2°	5.8° / 3.0°
DD/DA of FN-4	294.2° / 72.6°	300.1° / 76.5°	5.9° / 3.9°
DD/DA of FN-5	198.1° / 46.4°	187.6° / 47.2°	10.5° / 0.8°
DD/DA of FS-1	119.2° / 56.9°	123.5° / 53.2°	4.5° / 3.7°
DD/DA of FS-2	13.8° / 51.1°	16.8° / 56.2°	3.0° / 5.1°
DD/DA of FS-3	167.9° / 41.5°	172.5° / 39.2°	4.6° / 2.3°
DD/DA of FS-4	28.9° / 53.1°	31.8° / 49.6°	2.9° / 3.5°
TL of FR-1	8.95 m	9.23 m	0.28 m
TL of FR-2	9.25 m	8.67 m	0.58 m
TL of FR-3	9.76 m	10.13 m	0.37 m

Note: DD = dip direction, DA = dip angle, TL = trace length of fractures, FN-1,2…, FS-1,2… and FR-1,2…= ID-number of measured fractures

3.4 Pros and cons of the convergent photogrammetry method

Comparing to other methods, the presented method has the following pros and cons. The pros are:

1) It is fast to capture the required information (e.g. images and control points) for fracture mapping;
2) The fractures can be mapped without physically touching the rock face;
3) The fracture geometry is visually mapped from the images of the rock faces;
4) The instrument for in-situ fracture mapping is portable;
5) The recordings of the rock faces are preserved, so that it is possible to check and evaluate the mapping results later.

The cons of this method are:

1) Not all interesting target points can be captured, which depends on if the target points are identifiable in each image or not;
2) Low sampling speed for capturing a large number of target points;
3) The operator should have the background knowledge in photogrammetry;
4) It is difficult to measure the roughness of fracture surfaces. This could be overcome by automatic image matching of a great number of surface points.

4. 3-D laser scanner method

Three-dimensional (3-D) laser scanner is another tool for capturing geometrical information of the objects. With the improvement of resolution, measurement accuracy, scanning speed and lowering the cost, the 3-D laser scanner is now paid more attention for 3-D modelling and simulation in many industrial applications, such as surveying, robot navigation, architecture and car manufacturing. In rock engineering, the laser scanner has been applied to characterisation of roughness [38, 39] and tunnelling [40]. A new-mode 3-D laser scanner, Laser Radar (LARA), has recently been developed for 3-D characterisation of the objects [41, 42, 43]. This laser scanning system was used in this study to quantify fracture geometry from the exposed rock faces. The work presented in Paper C is summarised in this Chapter.

4.1 Laser radar (LARA) system

The LARA system was initially developed by Zoller + Fröhlich company (Wangen, Germany) for mobile robot navigation and inspection tasks. Because of the initial development purpose, the LARA system was designed for high-speed, high-performance and eye-safe scanning tasks, especially for medium-range applications in indoor and outdoor environments. Figure 23 shows the picture of LARA and two major components: the single-point laser measuring system (the lower-left part) and the mechanical beam deflection system (the upper-left part).

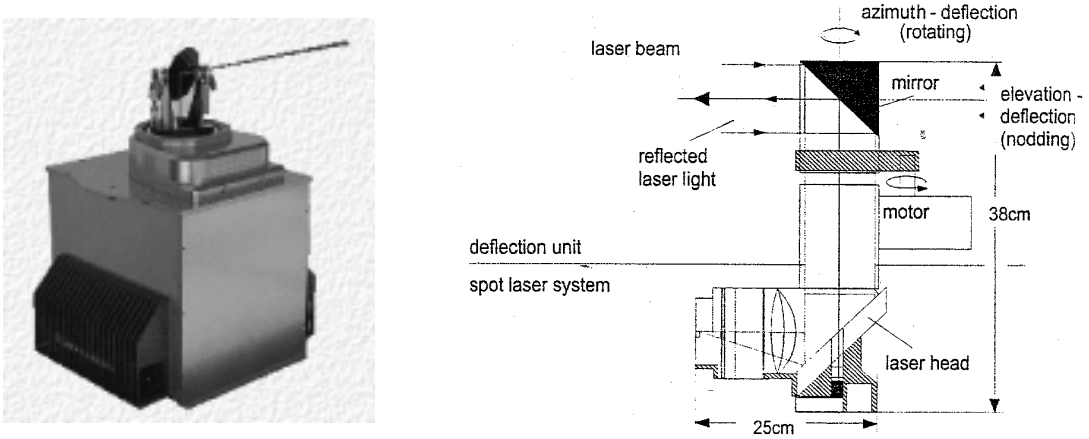

(a) (b)

Figure 23. LARA 3-D laser scanning system: (a) a picture of LARA instrument; (b) major components of LARA scanning system (from Z+F).

The point-sensor laser measurement system comprises the laser head, the high frequency unit and the signal processing unit for data pre-processing. This part controls the procedure of emitting, receiving and processing of the laser beam. By using the dual frequency AMCW (amplitude-modulated, continuous-wave) method in conjunction with a coaxial transmitter/receiver design, both range and reflectance of a target point can be obtained, and high measurement accuracy (within mm-range) can be achieved.

The mechanical beam deflection system consists of a special mirror and the motor control unit. The mirror is used for deflecting the emitted laser beam generated from the laser head at the bottom, and then collecting the back-scattered laser light cone. The motor control unit controls the mirror to rotate in the horizontal direction and nod in the vertical direction, which can make a scanning field overview of 360 degrees in azimuth and ±30 degrees in elevation.

Usually, the point-sensor laser scanner involves too much mechanical movement with lower scanning speed, which is not suitable for scanning a large object surface. However, the mechanical beam deflection system, specially designed in LARA, can greatly speed up the movement of the laser point. Therefore, it can quickly scan a large object surface, so that it is well suited for rock face mapping.

To obtain the 3-D co-ordinates of target points, both the range data captured by the single-point laser measurement system and the angular (horizontal and vertical) measurements created from the beam deflection system are used for computing the co-ordinates of the targets points.

Comparing with other laser scanners, LARA has some typical features suitable for fracture mapping at exposed rock faces: i) high-speed scanning with the data sampling rate up to 625 000 points per second; ii) the scanning range is 0.6 m – 54 m, which is a suitable distance in the most cases for fracture mapping from rock faces; iii) the mm-level accuracy (overall accuracy less than 15 mm) of LARA is acceptable for fracture mapping; iv) both 3-D co-ordinates and reflectance image of points are correspondingly recorded, which is special useful for viewing and interpreting properties of fracture geometry with the geologist's background knowledge and experience.

Table 4. Technical specifications of LARA systems

Accuracy data	**LARA25200**		**LARA53500**	
Ambiguity	0.6-12.6 m	0.6-25.2 m	0.6-26.8 m	0.6-53.5 m
Range resolution (mm/LSB)	0.38 mm		0.82 mm	
Angular accuracy (both azimuth and elevation)	0.05 ° (for imaging system) 0.08 ° (for profiling system)		0.05 °(for imaging system) 0.08 ° (for profiling system)	
Beam divergence	0.1/0.3 mrad		0.1/0.3 mrad	
Beam diameter	3 – 4 mm		3 – 4 mm	
Linearity error	≤ 3 mm		≤ 5 mm	
2σ noise f_s=125kHz X= 95% at distance D X= 5% at distance D	D = 13 m 3 mm 16 mm		D = 35 m 9 mm 47 mm	
Temperature drift (10°C – 40°C)	≤ 2 mm		≤ 4 mm	

Note: X(reflectivity) = P_R(received back-scattered laser light) / P_E(emitted laser light),
LSB = least significant bit, mrad = milliradians, f_s = signal frequency,

Two types of LARA systems are now available. Their technical specifications are listed in Table 4. In practice, the accuracy of fracture geometry measurements depends on not only the technical features of LARA systems but also other influential factors such as the characteristics of rock faces and fracture surfaces, position of the scanner and temperature. These factors need to take into consideration when conducting the fracture mapping work, which have been discussed in Paper D.

4.2 Procedure of fracture mapping by using LARA system

Fracture mapping by using the LARA system consists of the following four steps:
i) Control surveying by the TS; ii) Scanning the rock faces by the LARA system; iii) Transforming the laser scanning data to the TS co-ordinate system; iv) Quantifying fracture geometry from the recorded scanning data.

4.2. 1 Control surveying by using a non-reflector TS

The purpose of control surveying is: i) establishing a local co-ordinate system; ii) measuring several control points in order to register and transform different scanned parts of the rock face into the same co-ordinate system.

A non-reflector geodetic total station was used in this study for control surveying, due to the reasons such as: i) it is one of the most accurate instruments that are usually used in control surveying; ii) it is portable and suitable for *in-situ* mapping; iii) if it is inaccessible or dangerous for the operator to access the rock face, the target points can be measured without physically touching the rock face, because the non-reflector total station can take the object surface as a reflector.

When conducting the control surveying, it is important to make a careful designing in order to arrange the control points well distributed in the scanning areas of the rock face, and guarantee that there are at least three control points in each scanned area. To help the operator for well designing the control surveying and also for scanning, the pictures (it is better in colour) of the scanning parts must be taken before the control surveying and scanning steps. The control points must be easily recognised in the scanning images. In this case, it is better to put some markers on the control points if it is easy for the operator to access to the rock face, or select the identifiable points on the rock face.

4.2.2 Scanning the rock face by the LARA system

To measure fracture geometry with this method, the rock face is firstly scanned, and then the co-ordinates of the interesting target points are picked up for quantifying the geometrical parameters of fractures. The scanning procedure can be controlled by the scanning software, LaserRadar [44], which was associated with the LARA scanning system and developed by Zoller +Fröhlich company.

When scanning a rock face, it is important to guarantee the target area of the rock face can be covered by the LARA scanning. According to the scanning principle of LARA system, the single laser point is scanning from 0° to 360° in azimuth to finish one scan line, and then moves to the next scan line in elevation within ±30° with the horizontal and vertical rotation of the defection mirror (see Figure 24). So, the target area must be within this scanning scope, and also inside the range of the maximum reachable distance of the laser beam.

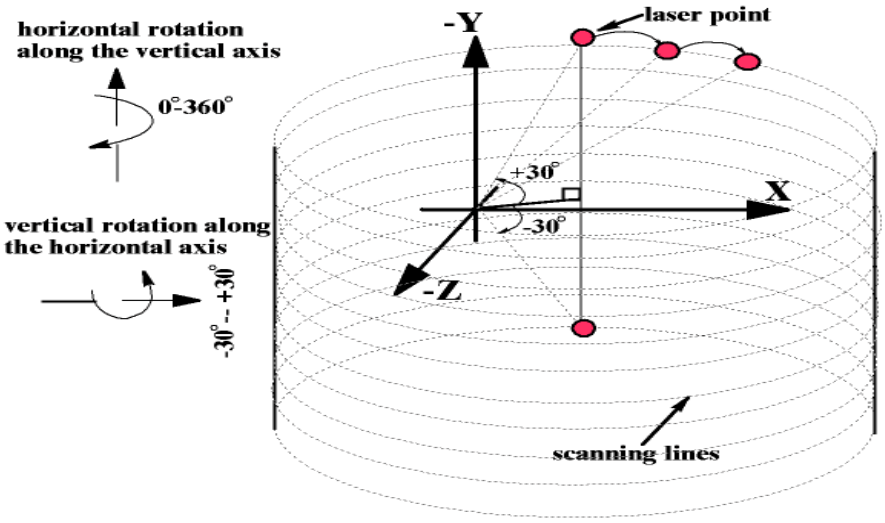

Figure 24. Scanning principle of LARA system.

However, the real covered area in each scanning also depends on the distance from the scanner to the rock face, and the geometry of the rock face such as the slope angle and the curvature of the rock face (see Figure 25).

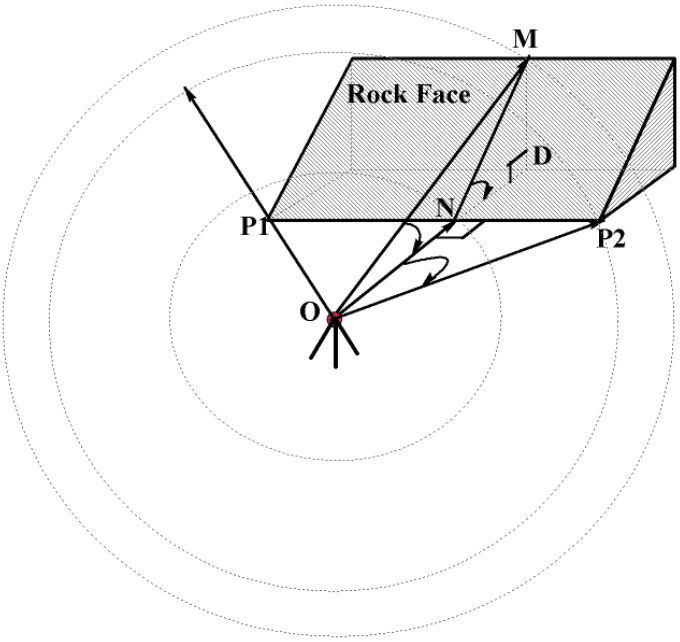

Figure 25. Scanning scope of a rock face by LARA system

Therefore, the real covered area in each scanning depends on the following five factors:
1) scanning overview field of LARA: 0° – 360° in azimuth and -30° – +30° in elevation;
2) ambiguity interval values of LARA, which are listed in Table 4;
3) normal distance from the scanner to the rock face;
4) slope angle of the rock face;
5) curvature of the rock face.

By taking consideration of these factors, the covered area can be roughly estimated. Figure 25 shows how the above-mentioned factors influence the covered area from each scanning. The dotted circles represent the scanning lines within different distances of the ambiguity intervals. The laser scanner is assumed to be located at the point O. OM is an ambiguity interval *AI*. ON is the normal distance *Dn* from the laser scanner to the rock face. The slope angle, e.g. ∠MND, is assumed as α. The scanning angle in elevation, e.g. ∠MON, is denoted by β, the positive value in the counter clockwise and the negative value in the clockwise. The covered area from each scanning can be roughly estimated by the length of MN and P_1P_2.

The distance *Dn* from the scanner to a rock face can be estimated by equation (10):

$$\begin{aligned} Dn &= OD - ND = OM\cos\beta - MD\cot\alpha = OM\cos\beta - OM\sin\beta\cot\alpha \\ &= OM(\cos\beta - \sin\beta\cot\alpha) = AI(\cos\beta - \sin\beta\cot\alpha) \end{aligned} \tag{10}$$

Since the ambiguity interval is known when using one of the LARA, and the maximum vertical scanning angle is ±30 degrees, then, OM=*AI*, β = 30°, and equation (10) becomes:

$$Dn = AI(\cos 30° - \sin 30°\cot\alpha) = AI(\frac{\sqrt{3}}{2} - \frac{1}{2}\cot\alpha) = \frac{AI}{2}(\sqrt{3} - \cot\alpha) \tag{11}$$

The length of MN can be calculated by equation (12):

$$\begin{aligned} MN &= \sqrt{OM^2 + ON^2 - 2*OM*ON*\cos\angle MON} \\ &= \sqrt{AI^2 + Dn^2 - 2*AI*Dn*\cos\beta} \\ &= \sqrt{AI^2 + \frac{AI^2}{4}(\sqrt{3} - \cot\alpha)^2 - 2*AI*\frac{AI}{2}(\sqrt{3} - \cot\alpha)*\cos 30°} \\ &= \frac{AI}{2}\sqrt{1 + \cot^2\alpha} \end{aligned} \tag{12}$$

The length of P_1P_2 is related to the size of the angle $\angle P_1OP_2$, which depends on *Dn*. The shorter the Dn, the larger the length of P_1P_2. In addition, the curvature of the rock face also affects the length of P_1P_2.

Therefore, the covered area from each scanning can be roughly estimated by the length of MN and P_1P_2 from equation (11) and (12). It is also indicated that the location of the scanner, which determines *Dn*, and the slope angle of the rock face are the most

influential factors related to the covered area from each scanning, as the scanning overview (both in azimuth and in elevation) and the ambiguity interval are fixed in the LARA system. To obtain a larger covered area from each scanning, the scanner must be properly placed by considering the slope angle of the rock face. If the rock face is steeper, the scanner must be placed a little bit far away from the rock face in order to cover the large length along the MN line. If the rock face is more flat, the scanner must be placed closer to the rock face to enlarge the length along the MN line. At the same time, the scanner should be located in a proper distance from the rock face in order to achieve a wide scope along the P_1P_2 line. In addition, the covered area can also be increased if lifting the scanner in height.

4.2.3 Transformation of the scanning data

The scanning data must be transformed into a known co-ordinate system for three purposes:
1) To determine the orientation parameters of fractures, e.g. dip direction and dip angle, the true north must be known. Since the true north is not indicated in the co-ordinate system of the LARA system, it is necessary to transform the laser scanning data into the total station co-ordinate system or a known true north co-ordinate system;
2) To cover the whole rock face, or a large part of the rock face, the scanner must move to different places and scan different parts of the rock face. In this case, the data of different scanned parts must be transformed and registered in one co-ordinate system;
3) To know the position and make a spatial analysis of fracture geometry in space, the scanning data have to be transformed to a known co-ordinate system.

To transform the laser data to the total station co-ordinate system, the non-reflector total station is used for the control surveying. At least three control points are measured in each scanning scope. In this study, more than four control points are usually captured in each scanning scope. And the co-ordinates of control points in both co-ordinate systems must be captured.

A three-dimensional similarity transformation model [36] is used for the transformation, and is expressed in equation (13):

$$\begin{bmatrix} X^t \\ Y^t \\ Z^t \end{bmatrix} = \begin{bmatrix} \delta x \\ \delta y \\ \delta z \end{bmatrix} + s * R(\alpha_1, \alpha_2, \alpha_3) * \begin{bmatrix} X^l \\ Y^l \\ Z^l \end{bmatrix} \tag{13}$$

where

X^t, Y^t, Z^t represent the co-ordinates in the total station co-ordinate system;
X^l, Y^l, Z^l represent the co-ordinates in the LARA co-ordinate system;
δx, δy, δz denote three translation parameters;
α_1, α_2, α_1 denote three rotation angles around the X-, Y- and Z-axis, respectively
s is the scale factor.

R stands for the total rotation matrix, which is the product of three separate rotation matrixes [45]:

$$\underset{3\times3}{R} = R(\alpha_1,\alpha_2,\alpha_3) = R_3(\alpha_3) * R_2(\alpha_2) * R_1(\alpha_1)$$

$$= \begin{bmatrix} \cos\alpha_3 & \sin\alpha_3 & 0 \\ -\sin\alpha_3 & \cos\alpha_3 & 0 \\ 0 & 0 & 1 \end{bmatrix} * \begin{bmatrix} \cos\alpha_2 & 0 & -\sin\alpha_2 \\ 0 & 1 & 0 \\ \sin\alpha_2 & 0 & \cos\alpha_2 \end{bmatrix} * \begin{bmatrix} 1 & 0 & 0 \\ 0 & \cos\alpha_1 & \sin\alpha_1 \\ 0 & -\sin\alpha_1 & \cos\alpha_1 \end{bmatrix} \quad (14)$$

Using Helmert method, seven transformation parameters, i.e. three translation parameters δx, δy, δz, three rotation parameters α_1, α_2, α_1 and one scale factor s, are first determined by using the two sets of co-ordinates of the control points in both LARA and total station co-ordinate systems. And then, the scanning data of other points can be transformed from the LARA co-ordinate system to the total station system. To do the transformation, a program was developed in this study. But the transformation can also be conducted by other commercial surveying programs, e.g. Geo12 [46] and LaraModel [47].

4.2.4 Quantifying fracture geometry from the recorded scanning data

To quantify fracture geometry parameters by using the presented method, 3-D co-ordinates of a set of target points are needed. After the rock face is scanned by the LARA system, co-ordinates of the target points can be semi-automatically captured. Since both range and reflectance intensity of the target points are simultaneously measured by LARA, the rock face is displayed in 2-D grey-scale image, and each point in the image is corresponded to its stored co-ordinates. By using the software LaserRadar [48], the target points can be picked up in two ways: i) pointing to the target points on the image one by one by using the mouse; ii) selecting a target area on the image by using the mouse (see Figure 26). Then, the 3-D co-ordinates of the corresponding points are saved in a data file for quantification of fracture geometry.

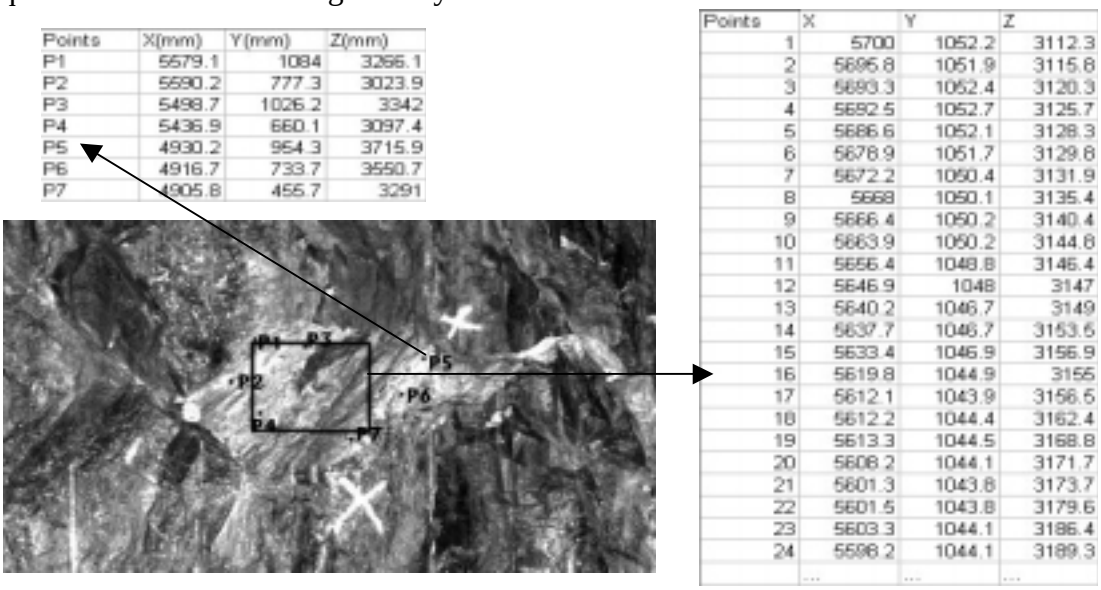

Figure 26. Capturing 3-D co-ordinates of target points by the help of a reflectance image.

The algorithms for computing the geometrical parameters of fractures, such as dip angle and dip direction, trace length, and spacing, will be presented in Chapter 5.

4.3 Case study

A case study was conducted at a rock face of Södra Länken, Stockholm in order to verify the presented mapping method. As Figure 27 shows, a non-reflector total station, Leica TCRM1002, was used for establishing a local co-ordinate system and measuring control points, and LARA scanner was used for scanning the rock face.

Figure 27. Scanning case study at a rock face of Södra Länken, Stockholm

The rock face is about 30 m × 9 m in area. The LARA scanner was placed about 5 m in front of the rock face, and positioned in four stations to scan the whole rock face. The maximum area of each scanning is about 14 m × 9 m. Each scanning takes about 5 min. The local oriented Cartesian co-ordinate with the known true north is established by using the total station and with the help of a compass. To transform the target points from the LARA co-ordinate system to the total station co-ordinate system and merge the four scanned parts together, more than six control points are measured by the total station in each scanned part of the rock face. Some markers are put on the rock face where is easy to access, and also some recognisable targets are selected as the control points on the rock face if it is difficult to reach physically. It takes about 10 min to establish the local co-ordinate system, and 3 seconds to measure each control point by the total station.

In this case study, orientation (dip direction and dip angle) and trace length of fractures were quantified by using both LARA scanner and the non-reflector total station for comparison of the measurement deviation between these two methods. The total station method for 3-D mapping of fracture orientation and trace length has been presented in

Chapter 2. When using LARA scanner to quantify these two parameters, a set of points along the trace line of a fracture or on a fracture surface are first captured from the scanning image by using the software LaserRadar, and then these parameters are computed from the recorded 3-D co-ordinates of these points by a program developed in this study. Measurements of orientation and trace length in the case study are listed in Table 5, with acceptable deviations, due mainly to the reasons such as the number and the position of captured target points, shape of the trace line and roughness of the fracture surfaces.

Table 5. Mapping results by total station and LARA system

Fractures	Total Station method		Laser-Radar method		Deviation:	
	DD/DA	TL	DD/DA	TL	Δ(DD/DA)	Δ(TL)
Fs-1	121/46		118/50		(3/4)	
Fs-2	087/54	8.67 m	079/48	8.57 m	(8/6)	0.10 m
Fs-3	119/51	9.23 m	125/47	9.12 m	(6/4)	0.11 m
Fs-4	126/52	10.13 m	131/54	10.07 m	(5/2)	0.06 m
Fs-5	078/72		083/75		(5/3)	
Fs-6	321/46	11.26 m	318/41	11.39 m	(3/5)	0.13 m
Fs-7	113/68		117/71		(4/3)	
Fs-8	066/76	6.78 m	071/78	6.86 m	(5/2)	0.08 m
Fs-9	167/53		161/51		(6/2)	

DD/DA= DipDirection/DipAngle; TL= TraceLength. Δ(DD/DA) and Δ(TL) = absolute deviation between Total Station method and Laser-Radar method.

4.4 Pros and cons of LARA system for fracture mapping

Comparing with other mapping methods, the advantages of the presented method are:

1) fast scanning speed, which permits us to scan a large area of rock faces;
2) the scanning distance of 0.6 m – 54 m and the wide scanning scope both horizontal and vertical directions are suitable for fracture mapping from rock faces;
3) the mm-level accuracy is enough for in-situ fracture mapping in the most of rock engineering applications;
4) both co-ordinates and images are correspondingly recorded, which is useful for virtual 3-D mapping of fracture geometry by utilising the human's experience and background knowledge;
5) it provides a good approach to copy the rock face in digital, visual and three-dimensional formats, especially in a known co-ordinate system, which is useful as a database for further analysis of fracture geometry and other applications.

The disadvantages of this method are:

1) it is costly for the instrument;
2) recording too many data if just for fracture mapping.

5. Quantification of fracture geometry

Geometrical parameters of fractures, such as orientation, spacing, trace length and roughness, actually represent a set of geometrical elements (e.g. plane, segment, line) and the relationship between these geometrical elements (e.g. angle between two planes or two vectors, distance between points). If the co-ordinates of a number of points are known, these geometrical elements and their relationship can be defined and determined. The previous Chapters have presented three methods, e.g. total station, close-range digital photogrammetry and 3-D laser scanner, for capturing the co-ordinates of the target points. The techniques for quantification of fracture geometry parameters are introduced in this Chapter based on both mathematical principles and their geological definition.

5.1 A new algorithm for computing orientation of fracture planes

To compute orientation of fracture planes from the recorded co-ordinates of target points, a new algorithm was developed and summarised here, and more detailed in Paper D.

Orientation of a fracture plane means the attitude of a fracture in space, which can be quantified in geology by three parameters: dip angle (DA), dip direction (DD) and strike (see Figure 2). DA, β ($0° \leq \beta \leq 90°$), is the downward-directed (positive) value of plunge measured in a vertical plane between a given line and the horizontal plane. DD, α ($0° \leq \alpha \leq 360°$), is the geographical azimuth, measured in clockwise rotation from north (0°), of the vertical plane containing the given line and corresponding to the direction of plunge of the line [3]. Strike is the azimuth of both directions of the intersection line between the fracture plane and the horizontal plane. Some geologists use strike of a fracture rather than DD, but this approach can introduce some ambiguity. In rock engineering, it is most usual to quote orientation data of a fracture by DD (three-digit value) and DA (two-digital value) separated by a slash, e.g. 035/70, 290/15 [49].

Although orientation parameters of a fracture are actually some angular quantities in the viewing of analytical geometry, cautions should be taken here that orientation parameters of a fracture are particularly defined in geology, which makes them as special angular quantities different from those usually defined in analytical geometry. So, the formulae from analytical geometry can not be directly used. The presented algorithm describes how to modify those available formulae from analytical geometry in order to compute fracture orientation correctly.

The presented algorithm depends upon some assumptions. These assumptions need to be designated first. Some notations related to the algorithm are also listed here.

Assumptions:

1) The referenced co-ordinate system is assumed to be as a right-hand Cartesian co-ordinate system. The positive X-axis directs to the true north, and the positive Y-axis points to the direction of counter clockwise rotation of 90 degrees from the positive X-axis; The X-Y plane is horizontal, and the positive Z-axis is upward;

2) Although a fracture surface is finite in size and non-planar, a best-fit plane of the fracture surface in a scale is usually used in geology to represent the orientation of the fracture surface. We assume the best-fit plane of the fracture surface is infinitely extended in three-dimensional space;
3) Fracture surface (F_s) and fracture plane (F_p) need to be distinguished in this paper. Fracture surface indicates a non-planar surface exposed at rock faces, but the fracture plane means an infinite best-fitting plane of the non-planar fracture surface, obtained from a set of measured points on the fracture surface.
4) In analytical geometry, the normal vector of a plane can be any vector vertical to the plane and starting from any point in space. Here, we define the normal vector of a plane as a vector being vertical to the plane, starting from the origin of the co-ordinate system, and pointing to the plane. Depending upon the pointing directions of the normal vector relative to the horizontal plane, we also define the upward normal vector ($\boldsymbol{n}^+$) and the downward normal vector ($\boldsymbol{n}^-$) of a plane. The former is pointing to the upper part of a horizontal plane, and the latter pointing to the down part of the horizontal plane (see Figure 28).

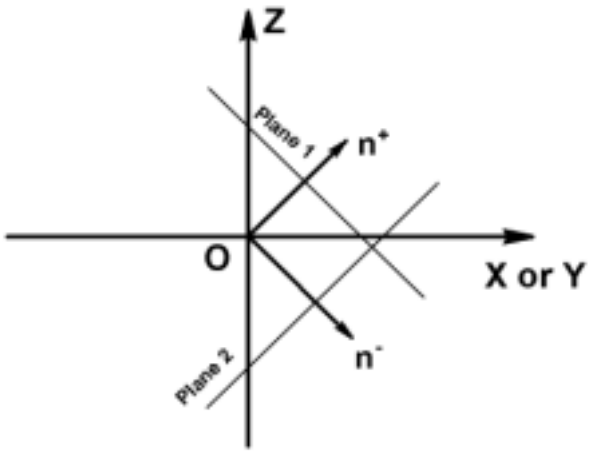

Figure 28. Definition of normal vector, upward normal vector and downward normal vector of a plane

Notations:

α -- dip direction (DD) of a fracture plane;
β -- dip angle (DA) of a fracture plane;
n – normal vector of a fracture plane;
$\mathbf{n_h}$ – horizontal component of **n**;
$\mathbf{n_v}$ – vertical component of **n**;
$\mathbf{n}^+$ -- the upper vector of **n**;
$\mathbf{n}^-$ -- the downward vector of **n**;
l – the line intersected between a fracture plane and the X-Y plane;
m – the vector of the maximum inclination line of the fracture plane;
$\mathbf{m_h}$ – the horizontal component vector of **m**;
φ -- angle between **n** and the positive X-axis;
κ -- angle between **n** and the positive Y-axis;
ω -- angle between **n** and the positive Z-axis;

P_i – the i-th target point captured from the fracture surface;
F_s – fracture surface;
F_p – fracture plane.

The main steps of the algorithm are summarised below:

1) Identifying target points captured from different fracture surfaces

The co-ordinates of target points measured from different fracture surfaces are usually stored together in one data file. So, the target points belonging to different fractures must be recognised automatically by the program. The easiest way to let the program identify the target points is to designate a special ID (IDentification) tag of the points measured from the same fracture surface. The point ID can be defined by the operator when the points are measured by the total station method or captured by photogrammetry and laser scanner methods.

2) Defining the best-fit plane of a fracture surface

A fracture surface exposed at rock faces is usually rough and wavy. So, orientation of a fracture is actually taken as the orientation of its best-fit plane. The best-fitting plane can be defined by using multiple regression method using co-ordinates of more than three non-collinear points, e.g. Pi (xi, yi, zi), i= 1, 2, … n, captured from the fracture surface. The best-fit plane equation of a fracture surface can be expressed as the equation of a regression plane:

$$Z = b_0+b_1X+b_2Y \tag{15}$$

The coefficients of this equation, b_0, b_1, b_2, can be obtained by solving the normal equations for the multiple regression with two independent variables, given by the method of least squares [50]:

$$\left\{\begin{array}{l} \sum_{i=1}^{n} z_i = nb_0 + b_1\sum_{i=1}^{n} x_i + b_2\sum_{i=1}^{n} y_i \\ \sum_{i=1}^{n} x_i z_i = b_0\sum_{i=1}^{n} x_i + b_1\sum_{i=1}^{n} x_i^2 + b_2\sum_{i=1}^{n} x_i y_i \\ \sum_{i=1}^{n} y_i z_i = b_0\sum_{i=1}^{n} y_i + b_1\sum_{i=1}^{n} x_i y_i + b_2\sum_{i=1}^{n} y_i^2 \end{array}\right\} \tag{16}$$

where n is the number of points captured from the same fracture surface; (x_i, y_i, z_i) are co-ordinates of the captured points (i=1, 2, … n).

Equation (16) can also be written in a matrix form:

$$\begin{bmatrix} n & \sum_{i=1}^{n} x_i & \sum_{i=1}^{n} y_i \\ \sum_{i=1}^{n} x_i & \sum_{i=1}^{n} x_i^2 & \sum_{i=1}^{n} x_i y_i \\ \sum_{i=1}^{n} y_i & \sum_{i=1}^{n} x_i y_i & \sum_{i=1}^{n} y_i^2 \end{bmatrix} \begin{bmatrix} b_0 \\ b_1 \\ b_2 \end{bmatrix} = \begin{bmatrix} \sum_{i=1}^{n} z_i \\ \sum_{i=1}^{n} x_i z_i \\ \sum_{i=1}^{n} y_i z_i \end{bmatrix} \tag{17}$$

or more simply written as:

$$\mathbf{Ax = W} \tag{18}$$

where the coefficient matrix $\mathbf{A} = [a_{jk}]$ is a 3x3 matrix,

$\mathbf{A} = \begin{bmatrix} a_{11} & a_{12} & a_{13} \\ a_{21} & a_{22} & a_{23} \\ a_{31} & a_{32} & a_{33} \end{bmatrix}$; $\mathbf{x}$, $\mathbf{w}$ are 3x1 column vectors, $\mathbf{x} = \begin{bmatrix} x_1 \\ x_2 \\ x_3 \end{bmatrix}$ and $\mathbf{w} = \begin{bmatrix} w_1 \\ w_2 \\ w_3 \end{bmatrix}$.

Comparing equation (17) with equation (18), the corresponding elements are:

$a_{11} = n$, $a_{12} = \sum_{i=1}^{n} x_i$, $a_{13} = \sum_{i=1}^{n} y_i$; $a_{21} = a_{12} = \sum_{i=1}^{n} x_i$, $a_{22} = \sum_{i=1}^{n} x_i^2$, $a_{23} = \sum_{i=1}^{n} x_i y_i$;

$a_{31} = a_{13} = \sum_{i=1}^{n} y_i$, $a_{32} = a_{23} = \sum_{i=1}^{n} x_i y_i$, $a_{33} = \sum_{i=1}^{n} y_i^2$;

$x_1 = b_0$, $x_2 = b_1$, $x_3 = b_2$; $w_1 = \sum_{i=1}^{n} z_i$, $w_2 = \sum_{i=1}^{n} x_i z_i$, $w_3 = \sum_{i=1}^{n} y_i z_i$

The three unknowns, b_0, b_1, b_2, can be obtained by solving equation (17) with either Gauss elimination or Cramer's theorem [51]. Then, occurrence of the best-fit plane in space depends on the properties, e.g. existence and uniqueness, of the solutions of equation (17). Two cases for the solution of equation (17) must be considered:

1) If D = 0, no solution for equation (17) or (18) can be obtained;
2) If D ≠ 0, equation (17) or (18) has precisely one solution. If using the Cramer's theorem, the solution of equation (17) or (18) are:

$x_1 = \frac{D_1}{D}$, $x_2 = \frac{D_2}{D}$, $x_3 = \frac{D_3}{D}$

where $D_1 = \begin{vmatrix} w_1 & a_{12} & a_{13} \\ w_2 & a_{22} & a_{23} \\ w_3 & a_{32} & a_{33} \end{vmatrix}$, $D_2 = \begin{vmatrix} a_{11} & w_1 & a_{13} \\ a_{21} & w_2 & a_{23} \\ a_{31} & w_3 & a_{33} \end{vmatrix}$, $D_3 = \begin{vmatrix} a_{11} & a_{12} & w_1 \\ a_{21} & a_{22} & w_2 \\ a_{31} & a_{32} & w_3 \end{vmatrix}$, $D = \begin{vmatrix} a_{11} & a_{12} & a_{13} \\ a_{21} & a_{22} & a_{23} \\ a_{31} & a_{32} & a_{33} \end{vmatrix}$.

These two cases indicate two types of spatial occurrences for the best-fitting plane of a fracture surface in space:

i) If D ≠ 0, the fracture plane is not vertical (either inclined or parallel) to the horizontal plane (e.g. the X-Y plane). The best-fit plane of a rock fracture surface can be defined. And then, dip angle and dip direction of the fracture plane can be determined.

ii) If D = 0, either the points captured from the fracture surface are collinear or the fracture plane is vertical to the X-Y plane and parallel to the Z-axis. The former case is impossible because we can make sure the points are non-collinear when capturing these points from the fracture surface. For the latter case, the best-fit plane can not be defined in this way. Actually in this case, the best-fit plane is not necessary for determining DA and DD. Obviously, DA is equal to 90 degrees. DD can be determined by defining a best-fit line of the captured points projected on the X-Y plane. This line can be obtained by using the linear regression with one independent variable. The regression equation can be expressed as:

$$Y=a+bX \tag{19}$$

The coefficients a and b of equation (19) can be obtained by the normal equations:

$$\begin{Bmatrix} n & \sum_{i=1}^{n} x_i \\ \sum_{i=1}^{n} x_i & \sum_{i=1}^{n} x_i^2 \end{Bmatrix} \begin{bmatrix} a \\ b \end{bmatrix} = \begin{bmatrix} \sum_{i=1}^{n} y_i \\ \sum_{i=1}^{n} x_i y_i \end{bmatrix} \tag{20}$$

or simply written as:

$$\mathbf{Bx = V} \tag{21}$$

where the coefficient matrix $\mathbf{B} = [b_{jk}]$ is a 2x2 matrix,

$$\mathbf{B} = \begin{bmatrix} b_{11} & b_{12} \\ b_{21} & b_{22} \end{bmatrix},\ b_{11} = n,\ b_{12} = \sum_{i=1}^{n} x_i,\ b_{21} = b_{12} = \sum_{i=1}^{n} x_i,\ b_{22} = \sum_{i=1}^{n} x_i^2;$$

x, **v** are column vectors, $\mathbf{x} = \begin{bmatrix} x_1 \\ x_2 \end{bmatrix}$ and $\mathbf{v} = \begin{bmatrix} v_1 \\ v_2 \end{bmatrix}$ respectively.

where $x_1 = a$, $x_2 = b$; $v_1 = \sum_{i=1}^{n} y_i$, $v_2 = \sum_{i=1}^{n} x_i y_i$.

$$x_1 = \frac{D_1}{D},\ x_2 = \frac{D_2}{D},\ D_1 = \begin{vmatrix} v_1 & b_{12} \\ v_2 & b_{22} \end{vmatrix},\ D_2 = \begin{vmatrix} b_{11} & v_1 \\ b_{21} & v_2 \end{vmatrix},\ D = \begin{vmatrix} b_{11} & b_{12} \\ b_{21} & b_{22} \end{vmatrix}.$$

The existence and uniqueness of solutions of equation (20) or (21) can also be discussed according to Cramer's theorem [51]. There are two cases:

i) If D = det **B** = 0, there are no solutions for equation (20) or (21). This means the best-fitting line is parallel to the Y-axis in the X-Y plane. Then, dip angle and dip direction of the fracture plane can be easily determined as 0° or 180°.
ii) If D = det **B** ≠0, there is precisely one solution for equation (20) or (21) according to Cramer's theorem [51]. In this case, a best-fit line can be defined, which can be used to determine dip direction of the fracture plane.

3) Determining DD and DA of fracture planes vertical to the X-Y plane

As discussed above, if det **A** = 0 in equation (17) or (18), the fracture plane must be vertical to the X-Y plane. So, DA of the fracture plane is equal to 90 degrees. To determine DD of the fracture plane, a best-fit line in X-Y plane is needed. But there are three cases (see Figure 29) in equation (20) or (21) necessary to be discussed:

Case 1: If det **B** = 0, the best-fit line is parallel to the Y-axis on X-Y plane. So, dip direction of the fracture plane can be determined: DD = 0° or 180°
Case 2: If det **B** ≠ 0 and b ≥ 0, then DD of the fracture plane can be determined by:
DD = 90° – arctan (b) (180/3.1415) or DD = [90° – arctan (b) (180/3.1415)] ±180°
Case 3: If det **B** ≠ 0 and b ≤ 0, then DD of the fracture plane can be determined by:
DD = [90° + arctan (b) (180/3.1415)] or DD = [90° + arctan (b) (180/3.1415)] ±180°

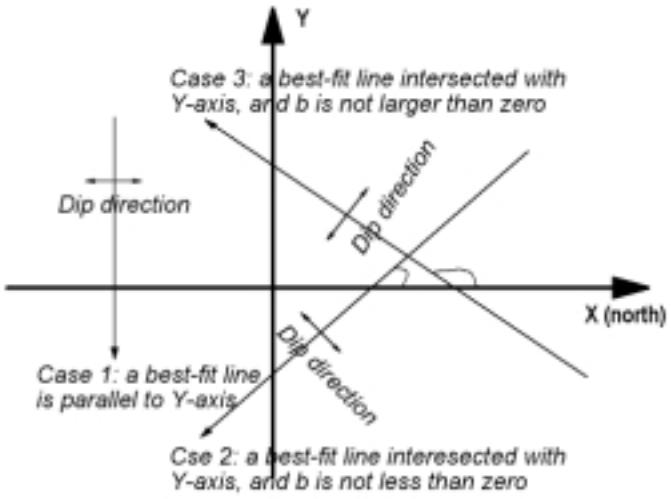

Figure 29. DD of fracture planes determined by three cases of a best-fit line on X-Y plane

4) Determining DD and DA of fracture planes not vertical to the X-Y plane

Fracture planes not vertical to the X-Y plane can be either parallel or inclined to the X-Y plane. These fracture planes can be defined by equation (15). A fracture plane in 3D space can also be expressed as a general form:

$$AX + BY + CZ + D = 0 \quad (22)$$

Comparing the coefficients of equation (15) and (22), the corresponding coefficients of these two equations are: $A = b_1$, $B = b_2$, $C = -1$, $D = b_0$. According to A, B, C and D, DA and DD of a fracture plane can be determined.

If A=0 and B=0, the fracture plane is parallel to X-Y plane, which is a horizontal fracture plane. So orientation of the fracture plane can be determined as:
DA = 0° and DD is not existed.

If $A \neq 0$ and $B \neq 0$, the fracture plane is inclined to X-Y plane. DA is actually the angle between a fracture plane and a horizontal plane (e.g. the X-Y plane), determined by the inner product of the unit vector, **k** (0,0,1), of the positive Z-axis and the normal vector, **n** (A, B, C), of the fracture plane:

$$\mathbf{k} \bullet \mathbf{n} = |\mathrm{k}|\,|\mathrm{n}|\cos\beta \tag{23}$$

$$\text{Then, } \cos\beta = \frac{\mathrm{k} \bullet \mathrm{n}}{|\mathrm{k}||\mathrm{n}|} = \frac{C}{\sqrt{A^2 + B^2 + C^2}} \tag{24}$$

According to the geological definition, DA, β ($0° \leq \beta \leq 90°$), is actually the acute angle between the fracture plane and a horizontal plane (e.g. the X-Y plane). But the angle calculated from equation (24) is in the range of 0-180 degrees. Therefore, DA should be determined by the following modified equation:

$$\text{DA} = \beta = \arccos\left|\frac{C}{\sqrt{A^2 + B^2 + C^2}}\right| \tag{25}$$

DD is actually an angle counted clockwise from the true north (i.e. the positive X-axis) to the horizontal component vector ($\boldsymbol{m_h}$) of the maximum inclination line (***m***) or the horizontal component vector ($\boldsymbol{n_h}$) of the normal vector (***n***) of the fracture plane (Fig. 30).

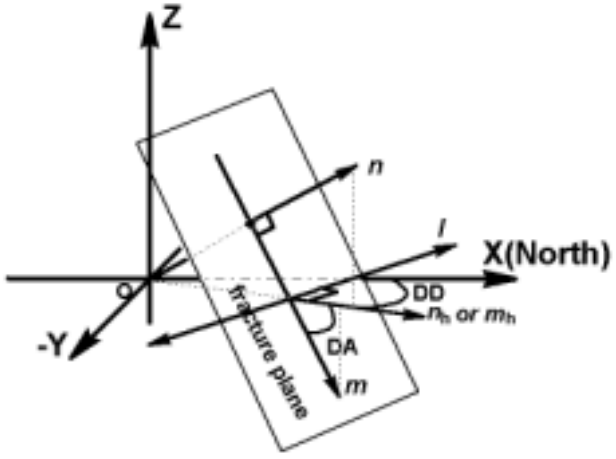

Figure 30. Determination of DD and DA of a fracture plane

The intersection line ***l*** between a fracture plane and the X-Y plane can be determined by:

$$\boldsymbol{l} \quad \begin{cases} AX + BY + CZ + D = 0 \\ Z = 0 \end{cases} \tag{31}$$

The directional values (p, q, r) of the intersection line ***l*** can then be given by:

$$p = \begin{vmatrix} B & C \\ 0 & 1 \end{vmatrix} = B, \qquad q = \begin{vmatrix} C & A \\ 1 & 0 \end{vmatrix} = -A, \qquad r = \begin{vmatrix} A & B \\ 0 & 0 \end{vmatrix} = 0.$$

Since the maximum inclination (plunge) line (***m***) of the fracture plane, the intersection line (***l***) and the normal vector (***n***) of the fracture plane are perpendicular to each other, ***m*** can be determined by using cross product of two vectors, ***l*** and ***n***:

$$\boldsymbol{m} = \boldsymbol{l} \times \boldsymbol{n} = \begin{vmatrix} i & j & k \\ p & q & r \\ A & B & C \end{vmatrix} = \begin{vmatrix} i & j & k \\ B & -A & 0 \\ A & B & C \end{vmatrix} \tag{32}$$

where ***i***, ***j***, ***k*** are unit component vectors of ***m***.

The horizontal component ($\boldsymbol{m_h}$) of ***m*** can be determined by simply projecting ***m*** onto the X-Y plane: $\boldsymbol{m_h}$ =[AC, BC, 0]= C*[A, B, 0]. DD of the fracture plane can be determined by the angle (α) between the positive X-axis and $\boldsymbol{m_h}$. This angle can be calculated using inner product of the unit vector of the positive X-axis, ***i*** [1, 0, 0] and $\boldsymbol{m_h}$ [AC, BC, 0]:

$$\boldsymbol{i} \bullet \boldsymbol{m_h} = |i| * |m_h| * \cos\alpha .$$

$$\text{Then, } \cos\alpha = \frac{i \bullet m_h}{|i| * |m_h|} = \frac{AC}{C * \sqrt{A^2 + B^2}} = \frac{A}{\sqrt{A^2 + B^2}} \tag{33}$$

There are several reasons due to the geological definition of DD while one must consider in finding DD:

1) DD is in the range of 0° – 360° according to its geological definition. But the angle (α) calculated from equation (33) is in the range of 0° – 180°;
2) DD is the angle counted clockwise from the positive X-axis (north) to $\boldsymbol{n_h}$ or $\boldsymbol{m_h}$. But the angle α derived from equation (33) might be counted from both clockwise and anticlockwise directions;
3) According to geological definition, DD of a fracture plane is actually determined by the upward normal vector of a fracture plane (see Figure 30). Depending upon the position of the fracture plane in a Cartesian co-ordinate system, the normal vector of a fracture plane can be either the upward or the downward. Therefore, DD calculated

from the upward normal vector will have a deviation of 180 degrees if calculated from the downward normal vector of the fracture plane (Figure 31).

Therefore, equation (33) needs to be modified in order to obtain a correct solution for determining DD of a fracture plane. The directional cosine values of the normal vector of a fracture plane can be used to determine which quadrants the normal vector is located in a Cartesian co-ordinate system, and also to identify if the normal vector is either the upward vector or the downward vector. They are given by:

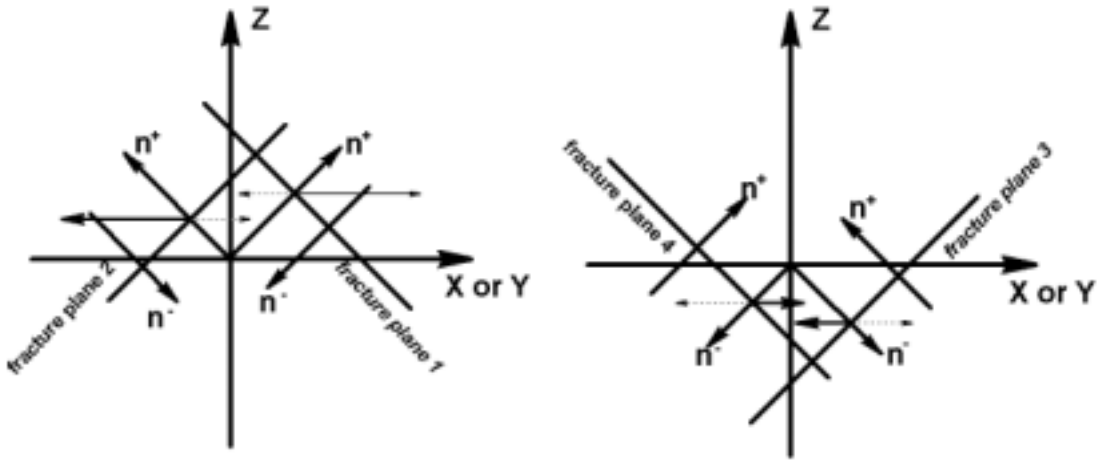

(a) (b)

Figure 31. Different locations of fracture planes in a Cartesian co-ordinate system

$$\left\{\begin{array}{l}\cos(\varphi)=\dfrac{A}{\pm\sqrt{A^2+B^2+C^2}}\\ \cos(\kappa)=\dfrac{B}{\pm\sqrt{A^2+B^2+C^2}}\\ \cos(\omega)=\dfrac{C}{\pm\sqrt{A^2+B^2+C^2}}\end{array}\right\} \quad (34)$$

where φ, κ, ω are the angles relative to the positive X-, Y-, Z-axis respectively. If D<0, $\pm\sqrt{A^2+B^2+C^2}$ takes "+" sign. If D≥0, $\pm\sqrt{A^2+B^2+C^2}$ takes "-" sign.

In order to obtain an angle within 0 and 90 degrees, equation (33) can be modified as

$$\alpha = \arccos\left(\left|\frac{A}{\sqrt{A^2+B^2}}\right|\right)*(180/3.14) \quad (35)$$

Then, DD of a fracture plane can be determined by the following rules:

$$\left\{\begin{array}{l} \text{i) if } \cos(\omega)\geq 0,\ \cos(\varphi)\geq 0, \text{ and } \cos(\kappa)\geq 0,\ DD = 360^\circ - \alpha; \\ \text{ii) if } \cos(\omega)\geq 0,\ \cos(\varphi)\geq 0, \text{ and } \cos(\kappa)< 0,\ DD = \alpha; \\ \text{iii) if } \cos(\omega)\geq 0,\ \cos(\varphi)< 0, \text{ and } \cos(\kappa)< 0,\ DD = 180^\circ - \alpha; \\ \text{iv) if } \cos(\omega)\geq 0,\ \cos(\varphi)< 0, \text{ and } \cos(\kappa)\geq 0,\ DD = 180^\circ + \alpha; \\ \text{v) if } \cos(\omega)< 0,\ \cos(\varphi)\geq 0, \text{ and } \cos(\kappa)\geq 0,\ DD = 180^\circ - \alpha; \\ \text{vi) if } \cos(\omega)< 0,\ \cos(\varphi)\geq 0, \text{ and } \cos(\kappa)< 0,\ DD = 180^\circ + \alpha; \\ \text{vii) if } \cos(\omega)< 0,\ \cos(\varphi)< 0, \text{ and } \cos(\kappa)< 0,\ DD = 360^\circ - \alpha; \\ \text{viii) if } \cos(\omega)< 0,\ \cos(\varphi)< 0, \text{ and } \cos(\kappa)\geq 0,\ DD = \alpha; \end{array}\right. \quad (36)$$

5.2 Spacing and trace length

Once the co-ordinates of target points are captured, spacing can be easily computed as the distance between each pair of immediately adjacent intersection points along a virtual scan-line, e.g. $P_i(x_i, y_i, z_i)$ and $P_{i+1}(x_{i+1}, y_{i+1}, z_{i+1})$ by:

$$\text{Spacing} = \sqrt{(x_i - x_{i+1})^2 + (y_i - y_{i+1})^2 + (z_i - z_{i+1})^2} \quad (37)$$

Trace length is the length of a fracture trace line which could be either a straight line or a curved line exposed at the rock face. If a trace line is almost straight, two points e.g. $P_1(x_1, y_1, z_1)$ and $P_2(x_2, y_2, z_2)$, at the ends of the trace line are measured. Then the trace length can be computed as the distance between these two points by:

$$\text{Trace length} = \sqrt{(x_1 - x_2)^2 + (y_1 - y_2)^2 + (z_1 - z_2)^2} \quad (38)$$

If the trace line is curved, a set of points, e.g. $P_1(x_1, y_1, z_1)$, $P_2(x_2, y_2, z_2)$, ……, $P_i(x_i, y_i, z_i)$, ……, $P_n(x_n, y_n, z_n)$ should be measured along the trace line. Then trace length can be computed as the sum of distances between each pair of immediately adjacent points by:

$$\text{Trace length} = \sum_{i=1}^{n} \sqrt{(x_i - x_{i+1})^2 + (y_i - y_{i+1})^2 + (z_i - z_{i+1})^2} \quad (39)$$

5.3 Roughness

Many researchers have developed different methods to characterize the surface roughness of natural rock fractures with different roughness parameters. These methods can be used to quantify the roughness of fracture surfaces from the recorded co-ordinate data. Since total station, laser radar and photogrammetric digital image matching can digitise a fracture surface both in profile and on the surface, the co-ordinate data of points captured by these methods enable us to quantify almost all fracture roughness parameters.

The methods range from simple measurements of amplitude, wavelength and slope, to more complex stochastic and frequency-domain analysis. Several commonly-used methods are summarised below:

1) JRC value

JRC (Joint Roughness Coefficient) is the most widely used roughness parameter proposed by Barton [52]. Barton and Choubey [53] investigated the roughness features of a large number of direct shear tests on natural fractures and calculated JRC values corresponding to the surface profiles of different specimens. Then, 10 typical roughness profiles are obtained. By comparing a roughness profile with these standard profiles, the JRC value of a fracture surface can be roughly estimated. If the co-ordinates of a number of points are digitised along a profile of a fracture surface, the curve of the profile can be obtained, and its JRC value estimated.

2) Amplitude parameters

The root mean square roughness (RMS) is a parameter of average deviation from the centreline [54]. The discrete form of RMS is:

$$RMS = \left[\frac{1}{n} \sum_{i=1}^{n} y_i^2 \right]^{1/2} \tag{40}$$

where n = number of evenly-spaced sampling points, y = amplitude of sampling point about centreline.

Two variations of RMS are:

- the centreline average (CLA) [54]:

$$CLA = \frac{1}{n} \sum_{i=1}^{n} |y|_i \tag{41}$$

- the mean square value (MSV) [55]:

$$MSV = \frac{1}{n} \sum_{i}^{n} y_i^2 \tag{42}$$

3) Wavelength parameters

- average spacing (A_r) is the average measured spacing between each adjacent peak;
- bearing length ratio (t_p) measures the proportion of the length of the profile that has positive amplitude values above a pre-selected vertical distance from the centreline;
- the method of peak counting [56] simply gives a count of the number of peaks per unit length.

4) Slope parameters

The root mean square (RMS) of the first derivative of the profile [57] is a parameter that characterizes a profile based on its average slope:

$$Z_2 = \left[\frac{1}{ndx^2} \sum_{i=1}^{n} (dy_i)^2 \right]^{1/2} \tag{43}$$

where n = number of evenly-spaced sampling points, dx = distance between points along sampling line, dy = distance between points normal to sampling line.

The root mean square (RMS) of the second derivative of the profile [57] is defined as:

$$Z_3 = \left[\frac{1}{n(dx_i - dx_{i-1})^2} \sum_{i=1}^{n} (dy_i - dy_{i-1})^2 \right]^{1/2} \tag{44}$$

A parameter Z_4 quantified the directionality of the roughness is defined as [57]:

$$Z_4 = \frac{\sum (dx_i)_p - \sum (dx_i)_n}{\sum (dx_i)_p + \sum (dx_i)_n} \tag{45}$$

where p = positive slope, n = negative slope.

5) Fractal dimension

Fractal theory [58] is useful for characterising the surface roughness of fractures. At least two parameters are needed to characterise a self-affine fractal object:

i) Fractal dimension *D*, which describes how roughness changes with scale;
ii) Amplitude *A*, which specifies the variance or surface slope at a reference scale.

The auto-correlation structure of a surface is captured by the fractal dimension *D*, or Hurst exponent *H* ($0<H<1$). The parameters *H* and *D* are related by the equation $H = E-D$, where *E* is the Euclidean dimension ($E = 3$ for a surface and $E = 2$ for a profile) for a self-affine fractal object. Since both the auto-correlation (i.e. *H* or *D*) and amplitude (*A*) of a surface contribute to the roughness of the surface, these parameters are used. To estimate *D* and *A*, several methods have been introduced in the literature, such as the variogram method [30], the structure function (SF) method [32], the spectral method [31], the roughness-length (RL) [33] and the line scaling method [59]. The application of the RL method is reported in Paper E.

6. Documentation of fracture mapping results

To make a full use of the information of fracture mapping for design and theoretical analysis in rock engineering, an effective documentation approach is necessary. The presented mapping methods create an opportunity to integrate different ways for documenting the fracture mapping information. Depending upon different applications, the following approaches can be applied for documentation.

1) Presenting fracture measurements as attributive tables and thematical diagrams

From the raw mapping data (e.g. the co-ordinates of target points), geological information exposed at rock faces can be listed in a table as attributive values of some geological quantities (e.g. trace length, dip angle and dip direction of fractures), and displayed as the thematical diagrams for statistical analysis and graphical display. Figure 32 shows an example to document orientation of fractures with an attributive table, a stereographic diagram and a rose diagram.

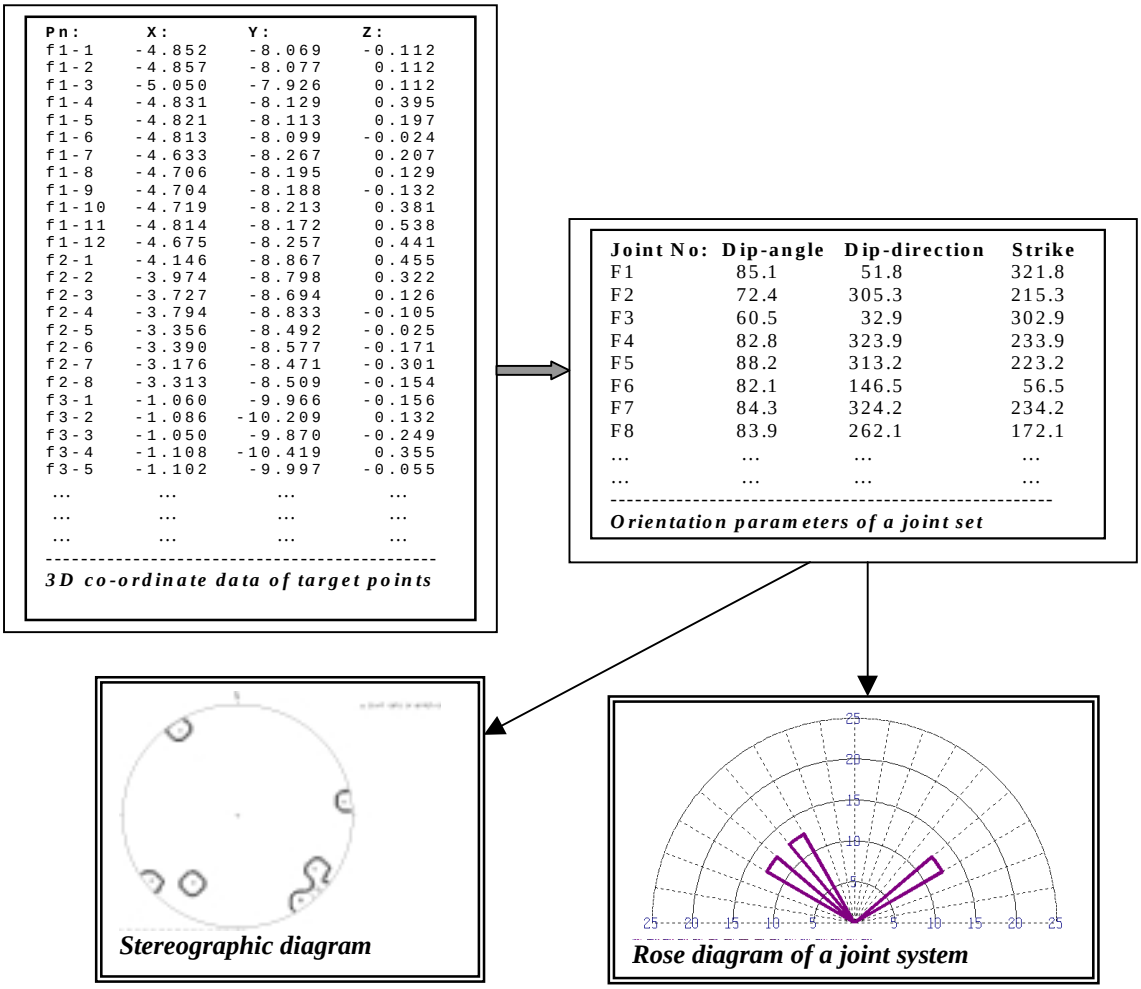

Figure 32. Presenting fracture information as attributive tables and thematical diagrams

This documentation method is often used in traditional mapping procedure. In this study, attributive tables and thematical diagrams can be created on-line and in-situ because the raw mapping data is captured and stored directly in digital form, and can be easily processed by a computer.

2) Displaying geological information with 2-D and 3-D graphics in a spatial co-ordinate system

Since the raw mapping data is captured in a 3-D co-ordinate system in this study, geological information can be displayed by 3-D graphics, and then be projected as 2-D graphics if necessary.

Figure 33 shows two examples. After a set of fracture planes and their orientation were determined by the recorded co-ordinates of a number of target points, the fracture planes were then displayed in a 3-D block within a reference co-ordinate system (Figure 33a). A large fracture surface (9 m x 2 m) was digitised in-situ with 10 cm interval by a non-reflector total station and then 3-D topography of the fracture surface was displayed in a spatial reference system for 3-D visual presentation of fracture roughness (Figure 33b).

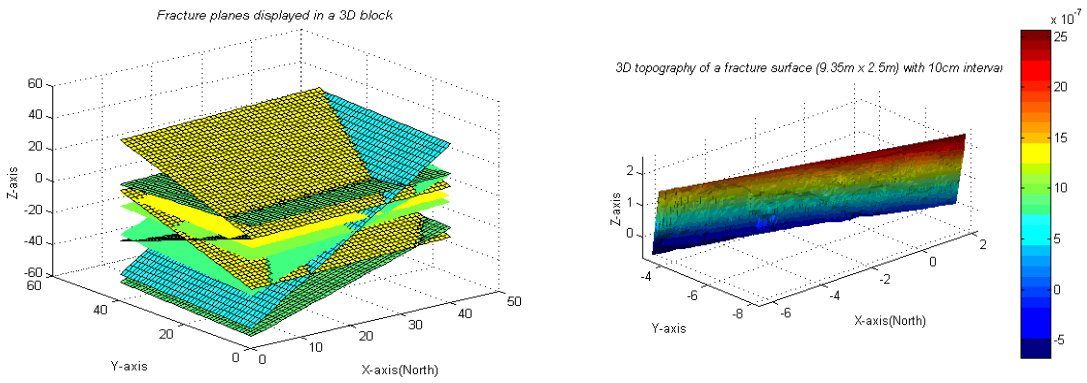

(a) (b)

Figure 33. Documentation of fracture geometry in 3-D graphics

3) Presenting geological information together with background images of rock faces

In some cases, it is better to overlay geological information onto the background images (or pictures) of rock faces. The visual information sometimes provides much more information than attributive values and thematical diagrams. Both photogrammetry and laser radar methods can provide this type of documentation. Figure 34 shows an example of photogrammetry method by presenting trace length of fractures in an image.

4) Providing primitive features for further 3-D geometrical and virtual modelling

Since the co-ordinates of 3-D target points together with images can be quickly captured by the laser radar, both geometrical and virtual modelling of fractures and other geological features from exposed rock faces become possible. Figure 35 shows a part of a rock face picked up as an image, 3-D point clouds and its 3-D textural model.

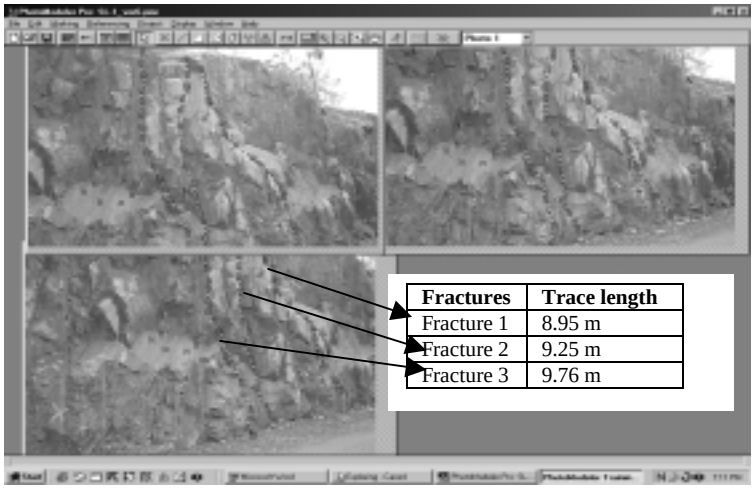

Figure 34. Geological information overlaid onto the background images of rock faces

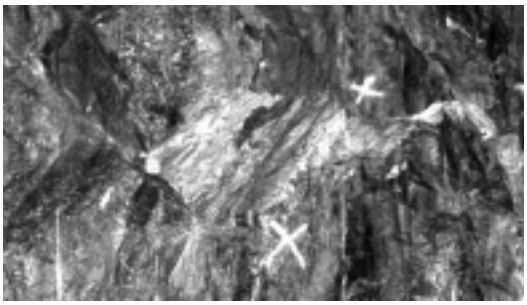

(a)

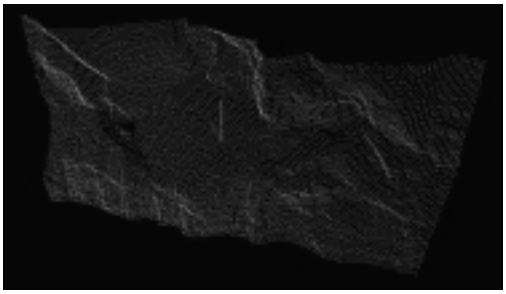

(b)

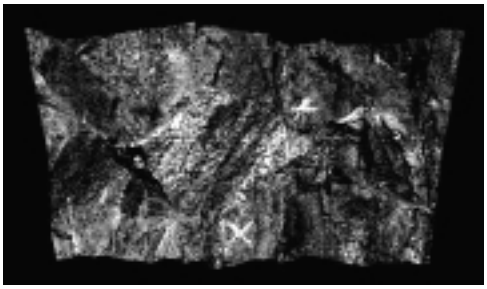

(c)

Figure 35. A rock face measured by LARA presented as an image (a), 3D point clouds (b) and 3D textual model (c)

7. Comparison of the three novel methods and the traditional method for rock fracture mapping

In this study, three novel methods, i.e. geodetic total station (TS), close-range digital photogrammetry (CRDP) and 3D laser scanner, Laser Radar (LARA), have been used for measuring fracture geometry at rock faces. Each method has both advantages and disadvantages for its application in a certain situation. For rock engineering applications, the pros and cons of the three methods and the traditional method are compared with each other by 14 items, which are the main points in the author's opinion (see Table 6).

Table 6. Assessment of different methods for fracture mapping at rock faces

Methods & their pros and cons	**Total Station**	**Close-Range Digital Photogrammetry**	**Laser Radar**	**Traditional Method**
Possibility for 3D mapping of:				
1) Orientation	4	4	4	5
2) Trace length	5	5	5	5
3) Spacing	5	5	5	5
4) Roughness	5	5	5	3
5) Ability for capturing data from rock faces	4	4	4	3
6) In-situ sampling speed	3	5	5	1
7) Automation of measurement	3	3	4	0
8) Accuracy of fracture mapping	4	4	4	2
9) Reliability of measurements	3	4	4	2
10) Independent of other methods	5	4	3	5
11) Recording format	3	4	5	1
12) Further use of recorded data	3	4	5	2
13) Cost of instruments	2	3	1	4
14) Requirement of special knowledge and training	3	2	3	4
Total assessment index:	**3.71**	**4.00**	**4.07**	**3.00**

To make a simple assessment of the 14 items, each item is given the same weight as others. Each item is subjectively ranked from 0 to 5 according to its contribution to rock engineering applications. Based on these rules, each item is firstly evaluated and given a grade, and then the grades of all 14 items for each method are summed and averaged, and expressed as average assessment number (AAN).

Applicability of a method for three-dimensional measurement of fracture geometry is the first important item to be evaluated because this is the basis for applying a new method in practice. There is a limit for the evaluated methods in Table 6 to measure orientation of a fracture plane if the fracture plane is hidden and only exposed as a straight line on the rock face. Then, the fracture plane can not be determined. But using the TM method, the operator can use a geological hammer to explore the fracture plane along the trace line, then the fracture orientation can be determined. From the author's experience, there are a few percentages of total fracture planes to be exposed on the rock faces as a straight trace line. In some cases, the fracture plane is exposed as a small facet on the rock face. Here it is quite risky to determine the fracture plane by the first three methods as well. In these cases, the TM method has an advantage over other methods. To measure roughness of

fracture surfaces, both TM and CRDP with convergent restitution techniques have some disadvantages than the other two methods. For instance, the fracture surface is more difficult to be evenly sampled by these two methods.

The first three methods can capture the data of fracture geometry without touching the rock face physically. Therefore, the fractures exposed in the inaccessible and dangerous rock faces can be measured more easily than with the TM method. But, not all fracture geometry exposed on the rock face can be measured by these methods because of the limits of scanning or sensing coverage from different directions and positions.

Sampling speed is another important factor for fracture mapping. The LARA method is the best choice in that respect. TS and CRDP methods need more time to pick up point by point and take enough images from different positions and directions. Sampling procedure with the traditional tools, e.g. a compass and measuring tape, is time-consuming.

Automation of measurement is an important factor to increase the amount of measurements of fracture geometry. Although it is difficult to measure fracture geometry fully-automatically, semi-automatic fracture mapping is reasonable. The LARA method, which can capture the co-ordinates of target points part by part, is more automatic than TS and convergent CRDP methods, which pick up the co-ordinates of target points one by one. But digital image matching from photogrammetric image pairs is possible to increase automation of measurement. With the TM method, measurement of fracture geometry is manual and slow.

Accuracy of the measurements of fracture geometry depends on many factors, but the important factor is the inherent features of the method. Using the TM method, the biased measurements are inevitable, and the apparent measurement of fracture orientation is difficult to avoid because the steepest inclination direction of a fracture plane is difficult to be determined. When using the photogrammetry method, the accuracy of measurements is very much dependent of the image quality and the identifiability of the target points from the images, which is one of the important drawbacks for the passive sensing methods. Total station and laser radar methods belong to the active sensing methods, so that the target points can be easily and accurately captured.

Reliability of the measurements is the ability to detect the presence of gross errors. The traditional method directly records the measurements of geometrical parameters fractures, but the other three methods compute the fracture parameters from the co-ordinates of target points. In this case, there is a higher probability to detect the gross errors when using the three novel methods. In addition, both photogrammetry and laser radar methods record not only co-ordinates of target points but also the images of rock faces, so that the redundant measurements are possible for detecting the reliability of the measurements.

Both CRDP and LARA methods need the control survey by using a total station in order to establish a local Cartesian co-ordinate system and register the images or different parts of scanning data. So, these two methods depend on the total station. But TS and TM

methods can be independently used for fracture mapping. A photogrammetric method using images taken from a stereo camera with a given base length would be independent of the total station if a local co-ordinate system is sufficient.

The recording format of the raw data and the measurements of fracture geometry will affect the automation of data processing and documentation in the subsequent mapping procedures. The three novel methods use the digital recording of the raw data, so that it is possible to quantify and analyse the fracture geometry automatically by using a computer. The CRDP method provides both data and images, which are useful for documentation as well. LARA method not only records data and images but also links the points in images to their 3D co-ordinates, so that the visual information can be corresponded to capture in 3D.

When the results of fracture mapping are used for the subsequent design work, additional information and measurements are needed, and the mapping results are required to be checked for the reliability and quality of the measurements. It is often difficult to check and reuse the measurements by the traditional method because the fracture parameters are recorded and presented in the notebook. Since the co-ordinates of target points are the raw data in TS method, it is possible to check the measurements. By using CRDP and LARA methods, the rock faces can be digitally presented in a known co-ordinate system. In this case, it is possible to check the measurements and obtain additional information. But for CRDP method, it is risky to extract the required 3D information if the target points are not identifiable on the images.

The cost of instruments also has an influence on the application of the methods. The instruments required for TS and LARA methods are expensive, compared with TM and CRDP methods.

The last factor to consider is the need for training a person to operate different fracture mapping methods. It is easy to operate the tools such as a compass and measuring tape for the TM method. Special training is necessary to be able to operate the TS and LARA methods. When using CRDP method for fracture mapping, special training and background knowledge on photogrammetry are needed.

In Table 6, the average assessment number shows the results of the ranking of different methods for rock fracture mapping. When selecting a method for fracture mapping, these or any other factors should be considered according to the requirements of different rock engineering applications.

8. Discussion

The presented three methods can be applied for semi-automatic measuring of the fracture geometry in three dimensions. Although measuring techniques of the three methods are different, the main steps for fracture mapping are common: first capturing the 3D co-ordinates of a number of target points, and then computing fracture parameters from the recorded co-ordinates of target points. To achieve successful results of fracture mapping, it is important to capture the co-ordinates of target points accurately and correctly. The accuracy of target point measurements for fracture mapping can be influenced by the following factors: i) accuracy and resolution of the instruments; ii) experience of the operator; and iii) features of the exposed rock faces or fracture surfaces. For fracture mapping of the rock face, the last factor is more important than the others. For instance, when using the TS method for fracture mapping, the properties of a fracture surface such as roughness, reflectance and inclination angle from laser beam to the surface will affect the measurements of the target points (Paper A and E). When using the convergent restitution techniques to capture co-ordinates of targets from images, the target points on the rock faces or fractures must be clearly recognised in different images (Paper B). Once the points are located on the edge of a surface, the mixed-pixel problems (Paper C) should be considered. In addition, if a fracture surface is hidden and exposed as a straight trace line on the rock face, the fracture orientation can not be determined because no points can be measured from the fracture surface. Thus, other methods should be used. A recent study by Post and Kemeny [16] proposed a method by using image processing techniques, Fisher distribution assumed for each fracture set and Monte Carlo simulation to determine the orientation of fractures particularly exposed in a straight trace line.

The TS is used not only for fracture mapping, but also for control surveying when applying CRDP and LARA methods. Therefore, the accuracy of fracture measurements by CRDP and LARA methods is also related to the accuracy of control points captured by the TS.

Mapping techniques can be classified into two categories, passive and active techniques, according to the types of sensors. The passive techniques, e.g. image processing and photogrammetry, capture the data of the objects passively, which means no energy is emitted for the purpose of sensing, only received. The active techniques, e.g. laser scanner and total station methods, obtain the information from the objects actively, which means that the properly formatted light or some other form of energy is emitted and then received once it has interacted with the objects. These two types of techniques have different applications according to the features of the objects. For fracture mapping on the rock faces, the passive methods have some problems to recognise the targets. For example: i) points without special features on the fracture surfaces are difficult to identify from different images; ii) it might be difficult to recognise if the variation of grey-level on the image is resulted by the boundary of a shadow or by the boundary of the gap between two walls of an open fracture that is recorded. The recognition of target points in images is dependent of the lighting conditions of the object, the resolution and contrast condition of the images With the active techniques, the geometry of fractures can be

easily captured. Stereoscopic evaluation of photogrammetric image pairs can significantly improve the possibility of recognization of target points.

Spatial analysis of fracture geometry is important for capturing the features of fractures at different parts of a rock mass and investigate the space-related properties of fracture geometry, such as the scale effect, heterogeneity and anisotropy of fracture roughness. With the development of the modern tools such as GPS (global positioning system), GIS (geographical information system), spatial characterisation of fractures and the rock mass structures becomes possible. Since the fracture geometry is captured and defined in a known co-ordinate system by the total station, it is possible to describe the position and features of fracture geometry in space. If GPS is used, the local co-ordinate system established by the total station can be linked to a global co-ordinate system (e.g. the national ground co-ordinate system or the global geographical co-ordinate system). Then, the fracture geometry in different rock masses can be correlated and quantified.

To speed up the mapping procedure and obtain large amount of fracture measurements, several research groups have made great efforts in trying to develop more automatic mapping of fracture geometry. In the author's opinion, semi-automatic techniques for fracture mapping on rock faces is the best choice due to the reasons such as: i) fracture mapping is not only a pure mapping activity, but also an interpretation procedure based on the operator's observation and geological background knowledge; ii) the fracture features exposed on the rock faces are too complicated to extract the useful information fully automatic. Therefore, semi-automatic techniques, like the presented three methods, can provide a means to utilise the human capacity for performing the intelligent mapping procedure of observing, interpreting and measuring. In addition, it can also leave the routine work to the computer and instruments for automatic operation.

9. Conclusions

Three novel methods, i.e. non-reflector total station (TS), close range convergent digital photogrammetry (CRDP) and laser radar (LARA), have been successfully applied for fracture mapping of exposed rock faces. Using these methods, four geometrical parameters of fractures, i.e. orientation, spacing, trace length and roughness, can be semi-automatically measured in three-dimensional space without need for touching the rock face physically.

The non-reflector TS is a useful tool for non-contact measurement of fracture geometry at a large distance from the rock faces, and for control surveying when CRDP and LARA methods are used for fracture mapping. The local co-ordinate system established by the TS can be linked to the existing co-ordinate systems by the known control points and GPS (Global Positioning System). Therefore, spatial analysis of fracture geometry in a known spatial reference is possible.

Convergent restitution techniques of photogrammetry can be applied to determine 3-D co-ordinates of target points on rock faces. This technique has been applied in this study. Since more than two images are used for restitution of the target position in space, a high degree of reliability, precision and accuracy of point measurements can be obtained. In addition, both metric and non-metric cameras can be used to capture the images around the rock faces. However, the target points on the rock faces must be clearly identified from each image. Otherwise, stereo restitution techniques are the best alternative.

Laser Radar (LARA) has some advantages compared with other methods for fracture mapping, such as high sampling speed with mm-level accuracy, large scanning distance, and recording of both 3-D co-ordinates and images of rock faces. If image segmentation techniques are used for processing the images captured by LARA, fracture geometry can be automatically characterised in three dimensions. In conclusion, integration of TS and LARA methods is to be found the best approach for fracture mapping of rock faces.

In this research work, the three methods (TS, CRDP and LARA) have been applied to fracture mapping of three rock faces at different sites in the Stockholm region. The accuracy of mapping results is acceptable for most rock engineering applications. Results of the case studies indicate that the accuracy of fracture measurements is influenced by several factors. Besides the resolution of instruments and experience of operators, geometrical features of fractures and rock faces (e.g. roughness and reflectance of fracture surfaces and inclination angle from laser beam to rock faces) have a great effect on the measurements of fracture geometry.

A new algorithm for computing dip direction and dip angle of rock fracture surfaces was developed in this study. The algorithm and codes can also be applied to determine orientation of any planes in space from the co-ordinates of more than three non-collinear target points.

For the presented methods, the procedure of fracture mapping can be divided into three major steps: 1) capturing the co-ordinates of a number of target points; 2) computing geometrical parameters of fractures from point co-ordinates; and 3) documenting results of fracture mapping. The first two steps are important to obtain accurate measurements of fracture geometry. The third step is needed for presentation of geometrical features of fractures together with other related information about the rock faces. The presented methods provide different ways for documentation of fracture mapping results, e.g. thematical tables and diagrams of fracture parameters, digital images (from CRDP and LARA), 3-D digital models (from LARA), 2-D and 3-D computer graphics (created by the co-ordinates of target points).

10. Suggestions for future work

Some future research works are suggested as follows:

1) Searching for more efficient techniques for 3-D automatic fracture mapping

Except for the presented three methods, there are also other approaches for 3-D mapping of object geometry, e.g. 3-D camera, computer vision and image processing techniques, and other types of laser scanners. Future research should try more techniques to compare their pros and cons of applicability for fracture mapping of rock faces.

2) Further investigation of the influences on fracture measurements

When using the presented three methods for fracture mapping, many factors can affect the fracture measurements. Although some factors on fracture measurements have been studied, more detailed investigation is needed for analysing the error propagation of different parameters of fracture geometry.

3) Integration of the presented methods with GPS and GIS for spatial analysis of fracture geometry in a spatial reference system

The presented methods provide an approach to quantify fracture geometry within a known co-ordinate system. Future development should try to link, by using GPS (Global Positioning System), the captured data by the presented methods to existing co-ordinate systems, e.g. the national ground co-ordinate system or the geographical co-ordinate system. Then, fracture geometry can be characterised in a real spatial reference, and may be useful for large scale engineering applications.

4) Utilisation of multiple media for visualisation of results

With the presented methods, fractures on the exposed rock faces can be recorded in many different ways, such as lists of co-ordinates of points, 2-D digital images, and 3-D digital models. Further work should apply different techniques, such as computer graphics, virtual reality modelling and image processing, to visualize geometrical features of fractures and geological information of rock faces.

5) Using the presented methods for other applications

The presented methods are also suitable for other 3-D mapping applications. So, the future study should explore the applicability to other rock engineering projects and other fields. One of such application is to use the geometry of fracture system established by these new methods for developing Discrete Fracture Network (DFN) models of rock masses which has a great potentiality in numerical analysis of rock engineering problems for performance and safety assessment of many facilities, such as underground nuclear waste repositories, oil/gas storage caverns, dam foundations, and geothermal energy extraction systems.

11. References

[1] Brown, E.T. (eds). 1981. Rock Characterization Testing and Monitoring: ISRM Suggested Methods. Pergamon Press Ltd, England.

[2] Hudson, J.A. 1989. Rock Mechanics Principles in Engineering Practice. CIRIA/Butterworths, London.

[3] Priest, S.D. 1993. Discontinuity Analysis for Rock Engineering. Chapman & Hall, London, UK.

[4] Reid, T.R., Harrison, J.P. 2000. A semi-automated methodology for discontinuity trace detection in digital images of rock mass exposures. Int J Rock Mech Min Sci 37: 1073-1089.

[5] Indraratna, B., Herath, A. and Aziz, N. 1995. Characterisation of surface roughness and its implications on the shear behaviour of joints. Mechanics of Jointed and Faulted Rock, Rossmanith (ed.), Balkema, Rotterdam, 515-520.

[6] Hakami, E. 1995. Aperture distribution of rock fractures. Ph.D. Thesis, Royal Institute of Technology, Stockholm, Sweden.

[7] Harrison, J.P. 1993. Improved analysis of rock mass geometry using mathematical and photogrammetric methods. Ph.D. Thesis, Imperial College, London, U.K.

[8] Rasouli, V., Harrison, J.P. 2000. Scale effect, anisotropy and directionality of discontinuity surface roughness. Proc. EUROCK Symposium, 50 Jahre Deutsche Gesellsehaft für Geotechnik e.V. Aachen, Germany. Balkema, Rotterdam, 751-756.

[9] Herda, H.H.W. 1999. Strike standard deviation for shallow-dipping rock fracture sets. Rock Mechanics and Rock Engineering 32 (4), 241-255.

[10] Baecher, G.B. 1972. Site exploration: a probablistic approach. PhD dissertation, Department of Civil Engineering, Massachusetts Institute of Technology, USA.

[11] Ross-Brown D.M., E.H. Wickens and J.T. Markland. 1973. Terrestial photogrammetry in open pits: 2-- an aid to geological mapping. Trans. Inst. Min. Metall., Section A, Min. Industry, 82, 115-130.

[12] Coe, J. A. 1995. Close-range photogrammetric geological mapping and structural analysis, Master thesis, Colorado School of Mines, USA.

[13] Beer, G., Oppiessnig, G., Golser, H., Fasching, A. and Gaich, A. 1999. Geotechnical data acquisition, numerical simulation and visualisation on site. Proceedings of the 9th ISRM Congress, Paris, A.A.Balkema, Rotterdam, 1333-1338.

[14] Wang, W. 1997. Computer vision for rock aggregates. Ph.D. Thesis, Royal Institute of Technology, Stockholm, Sweden.

[15] Hadjigeorgiou, J., Lemy, F., Côté, P. and Maldague, X. 2001. An evaluation of image analysis algorithms for constructing discontinuity trace maps. Submitted to Rock Mechanics and Rock Engineering.

[16] Post, R.M. and Kemeny, J.M. 2001. Image processing for automatic extraction of rock joint orientation data from digital images. Proc. The 38th US rock mechanics symposium, Washington D.C., USA, A.A.Balkema, Rotterdam (in press).

[17] Maerz, N.H., Franklin, J.A. and Bennett, C.P. 1990. Joint roughness measurement using shadow profilometry. Int. J. Rock Mech. Min. Sci. & Geomech. Vol. 27, No. 5, pp. 1073-1089.

[18] Bulut, F. and S. Tüdes. 1996. Determination of discontinuity traces on inaccessible rock slopes using electronic tacheometer: an example from the Ikizdere (Rize) Region, Turkey. Engineering Geology 44, 229-233.

[19] Ord, A. and C.C. Cheung. 1991. Image analysis techniques for determining the fractal dimensions of rock joint and fragment size distributions. In G. Beer, J.R. Booker and J.P. Carter (eds), Proceedings of the International Conference on Computer Methods and Advances in Geomechanics, Cairns. A. A. Balkema, Rotterdam, 87-91.

[20] Lanaro, F. 1999. A random field model for aperture and roughness of rock fractures. Licentiate thesis, Royal Institute of Technology, Sweden.

[21] Fadin, N. 2001. Scale dependency, heterogeneity and anisotropy of surface roughness of rock fractures. Licentiate thesis (in press), Royal Institute of Technology, Sweden.

[22] Moffitt, F.H. and Bossler, J.D. 1998. Surveying (Tenth Edition). Addison-Wesley Longman, Inc., Menlo Park, California, USA.

[23] Kavanagh, B.F. and Glenn, S.J. 1992. Surveying Principles and Applications (Third Edition), Prentice Hall, Englewood Cliffs, New Jersey, USA.

[24] Price, W.F. and Uren, J. 1989. Laser Surveying. Van Nostrand Reinhold (International) Co. Ltd., London, UK.

[25] Leica. 1998. Manual of Leica TCRM 1102.

[26] Spectra Precision AB. 1996. User's Manual of Geodimeter 468DR.

[27] Fan, H. 1997. Theory of Errors and Least Squares Adjustment. Lecture Notes, Division of Geodesy, Department of Geodesy and Photogrammetry, Royal Institute of Technology, Stockholm, Sweden.

[28] Svenska Byggnads Geodesi (SBG) AB. 1999. Manual of GeoPad.

[29] Leica. 1999. Manual of Leica TMS PROscan.

[30] Orey, S. 1970. Gaussian simple functions and Hausdorff dimension of level crossing. Z. Wahrscheinlichkeitstheor. Verw. Gebiete. 15:249-56.

[31] Berry, M.V., Lewis, Z.V. 1980. On the Weierstrass-Mandelbrot fractal function. R. Soc. London Proc. Ser. A. 370:459-84.

[32] Sayles, R. S., Thomas, T. R. 1977. The spatial representation of surface roughness by means of the structure function: a practical alternative to correlation. Wear. 42: 263-276.

[33] Malinverno, A. 1990. A simple method to estimate the fractal dimension of a self affine series. Geophys. Res. Lett. 17:1953-6.

[34] Siebrits, E., Smit, J.L., Ruther, H. & Malan, D.F. 1997. The mapping of blast-induced deformations in deep gold mines by digital photogrammetry. FRAGBLAST—International Journal of Blasting and Fragmentation 1; 233-242.

[35] Cooper, M.A.R. & Robson, S. 1996. Theory of close range photogrammetry, Close range photogrammetry and machine vision. Whittles Publishing. UK.

[36] Kraus, K. 1993. Photogrammetry. Ferd, Dümmlers Verlag, Bonn, Germany.

[37] Torlegård, K. 1967. On the determination of interior orientation of close-range cameras under operational conditions using three-dimensional test objects. Ph.D. thesis, Royal Institute of Technology, Stockholm, Sweden.

[38] Lanaro F., Jing L. and Stephansson O. 1998. 3D-laser measurements and representation of roughness of rock fractures, Mechanics of Jointed and Faulted Rock, Vienna, A.A. Balkema, Rotterdam, pp. 185-189.

[39] Fardin N., Stephansson O. and Jing L. 2000. Surface roughness and stationarity threshold of rock joints. Submitted to Int. J. Rock Mech. & Min. Sci.

[40] Hancock, J., Langer, D., Hebert, M., Sullivan, R., Ingimarson, D., Hoffman, E., Mattenleiter, M., Fröehlich, C. 1998. Active laser radar for high-performance measurements. Proceedings of the 1998 IEEE International Conference on Robotics & Automation, Leuven, Belgium.

[41] Mettenleiter, M., Härtl, F., Fröhlich, C., Langer, D. 2000. Imaging laser for 3-D modelling of real world environments. Proceedings of the IASTED International Conference Modelling, Identification and Control, Innsbruck, Austria.

[42] Langer, D., Mettenleiter, M., Härtl, F., Fröhlich, C. 2000. Imaging ladar for 3-D surveying and CAD modelling of real world environments. The International Journal of Robotics Research, Vol. 19, No. 11, 1075-1088.

[43] Fröhlich, C., Mettenleiter, M., Härtl, F., Dalton, G., Hines, D. 2000. Imaging laser radar for 3-D modelling of real world environments. Sensor Review, Vol. 20, No. 4, pp. 273-281.

[44] Zoller +Fröhlich GmbH. 2000. Manual of LaraRadar, Wangen, Germany.

[45] Fan, Theoretical Geodesy. 2000. TRITA GEOFO 2000:23. Lecture Book. Department of Geodesy and Photogrammetry, Royal Institute of Technology, Stockholm.

[46] SBG AB. 2000. Manual of Geo12, Stockholm, Sweden.

[47] Zoller +Fröhlich GmbH. 2001. Manual of LaraModel, Wangen, Germany.

[48] Zoller +Fröhlich GmbH. 2000. Manual of LaraRadar, Wangen, Germany.

[49] Brandy, B.H.G. and Brown, E.T. 1985. Rock Mechanics for Underground Mining. Allen & Unwin, London.

[50] Johnson, R.A. 1994. Miller & Freund's Probability & Statistics for Engineers (Fifth edition). Prentice-Hall, Englewood Cliffs, NJ.

[51] Kreyszig, E. 1993. Advanced Engineering Mathematics (Seventh Edition). John Wiley & Sons, Inc.

[52] Barton, N. 1973. Review of a new shear strength criterion for rock joints. Engineering Geology 7, 579-602.

[53] Barton, N. and Choubey, V. 1977. The strength of rock joints in theory and practice. Rock Mechanics 10, 1-65.

[54] Maerz N.H., Franklin J.A. and Bennett C.P. 1990. Joint roughness measurement using shadow profilometry. Int. J. Rock Mech. Sci. & Geomech. Abstr. 27: 329-343.

[55] Bendat, J.S. and Piersol, A.G. 1985. Random Data. Analysis and Measurement Procedures. Wiley, New York.

[56] Society of Automative Engineers (USA). 1986. Surface texture measurement of cold rolled steel. SAE Recommended Practice. SAE Handbook, Vol. 1, pp.9.01-9.03.

[57] Myers, M.O. 1962. Characterization of surface roughness. Wear 5, 182-189.

[58] Mandelbrot, B. 1982. The fractal geometry of nature. Freeman, San Francisco.

[59] Matsushita, M., Ouchi, S. 1989. On the self affinity of various curves. Physica D. 38:246-51.

[60] Feng Q. 1999. Geodetic total station for measuring geometry of discontinuities at exposed rock faces. Licentiate thesis. Royal Institute of Technology, Sweden.

[61] Imageware, Inc. 1999. Surfacer User's Guide, Ver. 9.0. Imageware, Inc., Ann Arbor, Michigan, U.S.A.

[62] Eos Systems Inc. 1996. PhotoModeler Pro User Manual Version 3.0. Eos Systems Inc. Vancouver, Canada.